ids, an effective nonviral vector [7]. Furthermore, quantitative comparison of transcriptional and post-transcriptional efficiency revealed that Ad vectors are 7000-fold more effective than cationic lipids for the transduction of nuclear DNA [8,9].

Transcription in mammalian cells is controlled by regulatory DNA sequences, including promoters, introns, and polyadenylation signals. An expression cassette, which is optimal, can be specific to each cell line or tissue [10–15]. It is therefore important to select an optimal expression cassette for each experimental model. Although Ad vectors are important in the basic studies of hepatocytes, the characteristics of the expression cassette of Ad vectors have not been fully determined in rodent primary cultured hepatocytes. In the present study, we investigated the ability of several promoters to mediate transgene activity by Ad vectors in mouse and rat primary hepatocytes.

2. Materials and methods

2.1. Isolation of hepatocytes from mouse and rat liver

Hepatocytes were isolated from male Sprague–Dawley rats and C57BL/6J mice (6 weeks old; Nippon SLC Co. Ltd., Kyoto, Japan) by the collagenase-perfusion method described by Seglen [16]. The cells were suspended in Williams' E medium containing 10% fetal calf serum, 1 nM insulin, and 1 nM dexamethasone. Next, cell viability was assessed by Trypan blue dye exclusion. Cells that were at least 90% viable were used in this study. For transfection, the suspended cells were seeded onto a 12-well plate at 2.5×10^5 cells/well. The cells were cultured in a humidified 5% CO_2 incubator at 37 °C.

2.2. Reverse transcription polymerase chain reaction (RT-PCR) analysis

The cells were harvested with a cell scraper. Total RNA was extracted from the cells with High Pure RNA Isolation Kit (Roche, Mannheim, Germany). RT-PCR was carried out using a TaKaRa RNA PCR kit (AMV) version 3.0 using an Oligo dT primer according to the manufacturer's instructions (TaKaRa, Shiga, Japan). Primers used here and the sizes of the putative PCR products are listed in Table 1. The PCR conditions were as follows: for mouse coxsackievirus and adenovirus receptor (CAR), 30 cycles of 45 s at 94 °C, 60 s at 57 °C, and 90 s at 72 °C; for mouse αv-integrin, 30 cycles of 45 s at 94 °C, 60 s at 56 °C, and 90 s at 72 °C; for mouse β3-integrin, 35 cycles of 45 s at 94 °C, 60 s at 53 °C, and 90 s at 72 °C; for mouse β5-integrin, 35 cycles for 45 s at 94 °C, 60 s at 57 °C, and 90 s at 72 °C; for mouse glyceraldehyde-3-phosphate dehydrogenase (GAPDH), 30 cycles of 45 s at 94 °C, 60 s at 57 °C, and 90 s at 72 °C; for rat CAR, 30 cycles of 45 s at 94 °C, 60 s at 53 °C, and 90 s at 72 °C; for rat αv-integrin, 30 cycles of 45 s at 94 °C, 60 s at 53 °C, and 90 s at 72 °C; for rat β3-integrin, 30 cycles of 45 s at 94 °C, 60 s at 53 °C, and 90 s at 72 °C; for rat β5-integrin, 30 cycles of 45 s at 94 °C, 60 s at 53 °C, and 90 s at 72 °C; for rat GAPDH, 30 cycles of 45 s at 94 °C, 60 s at 53 °C, 90 s at 72 °C.

2.3. Preparation of Ad vectors

Ad vectors were prepared by an in vitro ligation method as described previously [17,18]. First, shuttle vectors were constructed by the replacement of the cytomegalovirus (CMV) promoter in pHMCMV5 [19] with the Rous sarcoma virus (RSV) promoter, elongation factor 1α (EF) promoter (derived from pEF/myc/nuc; Invitrogen, Carlsbad, CA,

Table 1
Primers used in this study

Gene		Sequence (5′–3′)	Product size (bp)
Mouse CAR	Forward	TGATCATTTTGTATTCTGGA	211
	Reverse	TTAACAAGAACGGTCAGCAG	
Mouse αv-integrin	Forward	CCAGCCTGGGATTGTAGAAG	105
	Reverse	ACTCCAGTGGGTCATCTTTG	
Mouse β3-integrin	Forward	TCTGGCTGTGAGTCCTGTGT	115
	Reverse	GCCTCACTGACTGGGAACTC	
Mouse β5-integrin	Forward	TCGTGTGAAGAATGCCTGTT	126
	Reverse	GCTGGACTCTCAATCTCACC	
Mouse GAPDH	Forward	ACCACAGTCCATGCCATCAC	452
	Reverse	TCCACCACCCTGTTGCTGTA	
Rat CAR	Forward	ATGGATCCTACACCCGAACAGAGGATCG	280
	Reverse	GCGATTTCGCGTCGCCAGACTTGACAT	
Rat αv-integrin	Forward	GGGCTACATCCTAGGCCTTC	273
	Reverse	GAAGATTCCAGGCAACAGGA	
Rat β3-integrin	Forward	CATCACGTCGCAGAACATCT	279
	Reverse	CTTGGTGGCCGTGTACTTCT	
Rat β5-integrin	Forward	TGTGTCTCTGCGGTGTTTGC	312
	Reverse	CCACGAGAACACCACAACAA	
Rat GAPDH	Forward	GGTCGGTGTGAACGGATTTG	298
	Reverse	GTGAGCCCCAGCCTTCTCCAT	

USA), or β-actin promoter/CMV enhancer (CA) promoter (kindly provided by Dr. J. Miyazaki, Osaka University, Japan) [20], resulting in pHMRSV5, pHMEF5, and pHMCA5, respectively. The β-galactosidase (LacZ) gene was derived from pCMVβ (Marker Gene, Inc., Eugene, OR, USA) and inserted into pHMCMV5, pHMRSV5, pHMEF5, and pHMCA5, resulting in pHMCMV5-LacZ, pHMRSV5-LacZ, pHMEF5-LacZ, and pHMCA5-LacZ, respectively. Next, I-CeuI/PI-SceI-digested shuttle vectors were ligated with I-CeuI/PI-SceI-digested pAdHM4 [19], resulting in pAd-CMV-LacZ, pAd-RSV-LacZ, pAd-EF-LacZ, and pAd-CA-LacZ, respectively. To generate Ad vector particles, the Ad vector plasmids were digested with PacI, and the resulting digested Ad vector plasmids were transfected into 293 cells with Superfect according to the manufacturer's protocol (Qiagen, Inc., Valencia, CA, USA). Each Ad vector was purified by $CsCl_2$ step gradient ultracentrifugation, followed by $CsCl_2$ linear gradient ultracentrifugation. The concentration of vector particles was determined by a spectrophotometric method [21].

2.4. LacZ assay

After 24 h of isolation, the hepatocytes seeded onto a 12-well plate were treated with each Ad vector for 1.5 h. Next, the cells were washed with culture medium and then cultured for an additional 48 h. For 5-bromo-4-chloro-3-indolyl-β-D-galactopyranoside (X-gal) staining assays, the cells were washed with phosphate-buffered saline, fixed with 0.5% glutaraldehyde, and stained with X-gal solution (1.3 mM $MgCl_2$, 15 mM NaCl, 44 mM HEPES, 3 mM potassium ferricyanide, 3 mM potassium ferrocyanide, and 0.05% X-gal). The β-galactosidase activity was quantitatively measured with a Luminescent β-Gal Kit (Clontech, Palo Alto, CA, USA) according to the manufacturer's protocol, and the activity was normalized by the cell number.

3. Results

Ad vectors infect target cells in two steps: (i) attachment of the vector to the cells via the knob domain to CAR on the cell membrane and (ii) internalization of the vector into the cell by interaction with Arg-Gly-Asp motifs of penton base with αvβ3- and αvβ5-integrins on the cell membrane [22–25]. Thus, the expression of CAR and integrins mediates gene transfer by the Ad vector. To examine the use of Ad vectors in hepatocytes, we first confirmed that the cells express these receptors by RT-PCR. As shown in Fig. 1, CAR, αv-integrin, β3-integrin, and β5-integrin were expressed in mouse primary hepatocytes, and CAR, αv-integrin and β5-integrin were expressed in rat primary hepatocytes.

To compare promoter strength, we constructed four Ad vectors containing LacZ as a reporter gene driven by the RSV, EF, CMV, or CA promoter (Ad-RSV-LacZ, Ad-EF-LacZ, Ad-CMV-LacZ, or Ad-CA-LacZ, respectively). We infected primary mouse and rat hepatocytes with each Ad vector at 300 vector particles (VP)/cell, and we checked

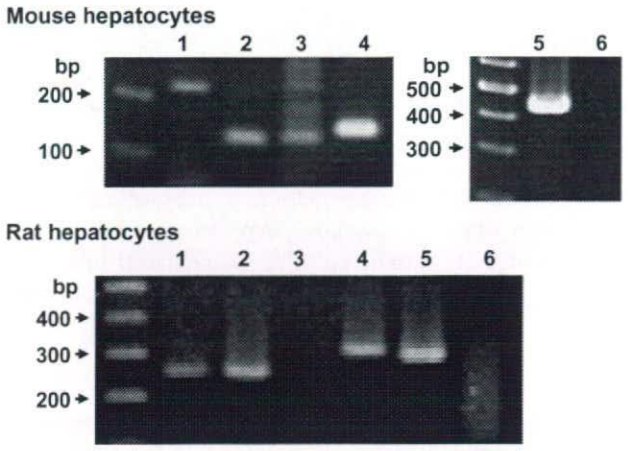

Fig. 1. RT-PCR analysis of receptors for Ad vectors. Total RNA was isolated from hepatocytes, purified with High Pure RNA Isolation Kit, and amplified by RT-PCR. Upper and lower panels are the data from mouse and rat hepatocytes, respectively. The left-most lane shows a 100-bp ladder, and the other lanes are as follows: lane 1, CAR; lane 2, αv-integrin; lane 3, β3-integrin; lane 4, β5-integrin; lane 5, GAPDH; lane 6, sample lacking reverse transcription. GAPDH was used as an endogenous control.

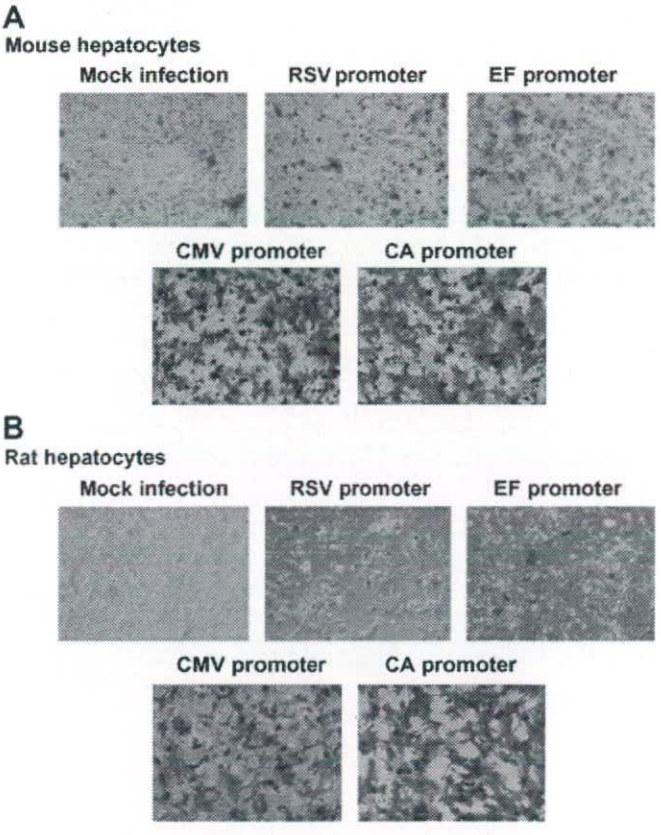

Fig. 2. X-gal staining of Ad vector-transduced rodent primary hepatocytes. Primary cultured hepatocytes isolated from the livers of mouse (A) and rat (B) were seeded onto 12-well plates. The cells were transfected with Ad-RSV-LacZ, Ad-CMV-LacZ, Ad-CA-LacZ, or Ad-EF-LacZ at 300 VP/cell for 1.5 h. The cells were washed with culture medium, cultured for an additional 48 h, fixed, and stained with X-gal.

the transduction of LacZ into the cells by staining them with X-gal after 48 h of transfection. As shown in Fig. 2, the cells infected with Ad-CA-LacZ or Ad-CMV-LacZ

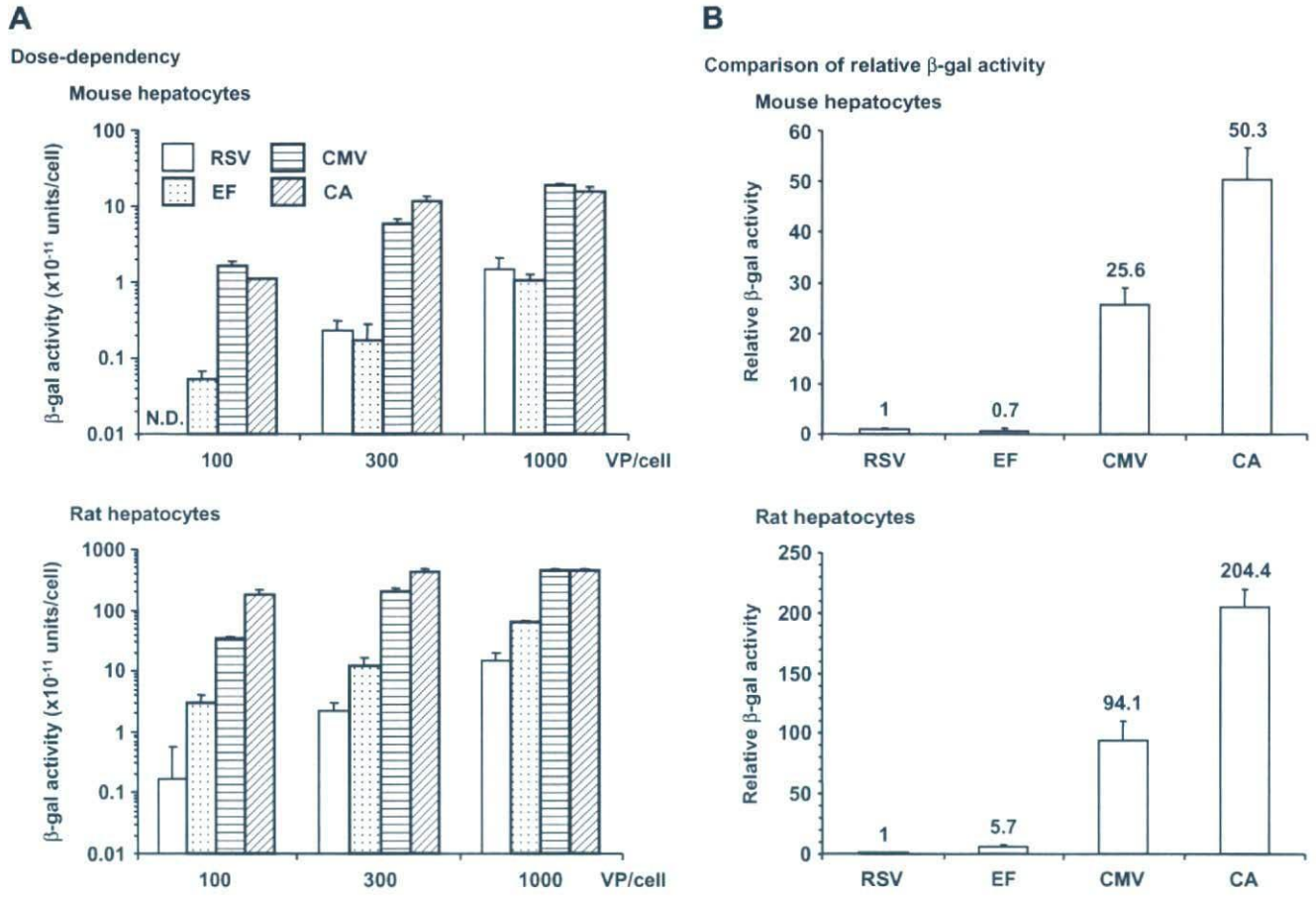

Fig. 3. Dose-dependent transduction activity in Ad vector-transduced rodent primary hepatocytes. (A) Dose-dependence of Ad vectors on transgene activity. Mouse and rat primary hepatocytes were treated with the indicated Ad vectors at the indicated concentration for 1.5 h. After washing with medium, the cells were cultured for 48 h and then harvested for the measurement of β-galactosidase (β-gal) activity using a luminescence assay kit. β-gal activity was normalized by the number of cells. (B) Comparison of relative transgene activity. The β-gal activity of each Ad vector at 300 VP/cell was expressed relative to the activity of Ad-RSV-LacZ. The numbers above each column indicate the relative β-gal activity. Data are means ± SD ($n = 3$). N.D., not detected.

were stained with X-gal, but few of those infected with Ad-RSV-LacZ or Ad-EF-LacZ were stained (Fig. 2A and B). Most of the hepatocytes were stained with X-gal when they were infected with Ad-CA-LacZ or Ad-CMV-LacZ at 1000 VP/cell (data not shown).

Next, to evaluate the dose-dependence of Ad vector efficiency, we measured β-galactosidase activity in cells infected at 100, 300, and 1000 VP/cell. The β-galactosidase activity increased in a dose-dependent manner for each of the Ad vectors in both mouse and rat hepatocytes (Fig. 3A), but the transcriptional activities differed among the promoters. Fig. 3B shows the β-galactosidase activity for each of the promoters relative to Ad-RSV-LacZ in cells infected at 300 VP/cell. The CA promoter had the highest transcriptional activity (50.3- and 204.4-fold in mouse and rat hepatocytes, respectively).

4. Discussion

Ad vectors have been widely used in basic and clinical studies of the liver, and liver function is often investigated using primary hepatocytes isolated from mouse and rat. However, there is little information on Ad vector-mediated gene expression in primary hepatocytes. In the present study, we evaluated the use of Ad vectors with several different promoters for transfecting rodent primary hepatocytes. We found that the CA promoter mediates strong transcriptional activity.

The first step for the expression of genes in mammalian cells is the binding of transcriptional factors to the promoter sequence upstream of the genes. This binding of transcriptional factors differs according to the promoter sequences. For example, Ad vectors with the CMV and EF promoters have very low and high transduction efficiency, respectively, in mouse embryonic stem cells [18]. In contrast, we found here that an Ad vector with the CMV promoter effectively expressed the LacZ gene in rodent hepatocytes, but they did not when they had the EF promoter. These different promoter activities suggest that different transcriptional factors participate in gene expression by mouse embryonic stem cells and mouse primary hepatocytes. Furthermore, the similar profiles of promoter strength in mouse and rat hepatocytes suggest that the two cell types utilize similar transcription factors.

In vivo studies in mice have shown that the CMV promoter has 4- to 10-fold higher transcriptional activity than the CA promoter in the liver [13], but in the current study, the CA promoter was approximately 2-fold more effective than the CMV promoter in rodent primary hepatocytes. This discrepancy might be due to the distribution of Ad vectors in the in vivo assay. Because systemically administrated Ad vectors distribute into parenchymal and nonparenchymal cells, the transgene activity may reflect the transcription of genes in not only hepatocytes but also Kupffer, stellate, and sinusoidal endothelial cells [26–28]. These nonparenchymal cells play important roles in hepatic processes, and the optimization of their transcriptional cassette is of interest for future studies. Another possible explanation for the difference in the in vitro and in vivo results is a difference in transcriptional factors between intact and primary hepatocytes. Indeed, the isolation of hepatocytes induces a prompt decline in certain liver-specific genes [6].

The expression of genes in mammalian cells is controlled by biochemical machinery including the promoter, enhancer, intron, and polyadenylation (PA) signal. To compare promoter activity, we added the PA signal of bovine growth hormone. Further, the optimization of the enhancer, intron, and PA signal is needed to prepare an ideal Ad vector for hepatocytes. The regulation of expression levels is also important for investigations using transgenes, and various systems have been developed for this purpose [29–32]. Xu et al. developed regulated transgene systems based on Ad vectors using elements that can be controlled by tetracycline, ecdysone, and antiprogestin [33]. Although these controllable systems are useful for basic research in rodent primary hepatocytes, chemical reagents must be added to regulate the gene expression. In the present study, we developed Ad vector systems regulated by several promoter sequences, and we found that the expression can differ by as much as 1000-fold according to the promoter sequence and the concentration of the Ad vector used to infect the rodent primary hepatocytes. The different expression profiles for each Ad vector showed to be useful for further basic hepatology research.

Acknowledgements

We thank Mrs T. Suzuki, R. Okude, and S. Matsukawa for their technical supports and helpful comments.

References

[1] G. Elaut, T. Henkens, P. Papeleu, S. Snykers, M. Vinken, T. Vanhaecke, V. Rogiers, Molecular mechanisms underlying the dedifferentiation process of isolated hepatocytes and their cultures, Curr. Drug Metab. 7 (2006) 629–660.

[2] A. Guillouzo, Liver cell models in in vitro toxicology, Environ. Health Perspect. 106 (Suppl. 2) (1998) 511–532.

[3] D.A. Casciano, Development and utilization of primary hepatocyte culture systems to evaluate metabolism, DNA binding, and DNA repair of xenobiotics, Drug Metab. Rev. 32 (2000) 1–13.

[4] E.L. LeCluyse, Human hepatocyte culture systems for the in vitro evaluation of cytochrome P450 expression and regulation, Eur. J. Pharm. Sci. 13 (2001) 343–368.

[5] R. Gebhardt, J.G. Hengstler, D. Muller, R. Glockner, P. Buenning, B. Laube, E. Schmelzer, M. Ullrich, D. Utesch, N. Hewitt, M. Ringel, B.R. Hilz, A. Bader, A. Langsch, T. Koose, H.J. Burger, J. Maas, F. Oesch, New hepatocyte in vitro systems for drug metabolism: metabolic capacity and recommendations for application in basic research and drug development, standard operation procedures, Drug Metab. Rev. 35 (2003) 145–213.

[6] C. Guguen-Guillouzo, P. Gripon, Y. Vandenberghe, F. Lamballe, D. Ratanasavanh, A. Guillouzo, Hepatotoxicity and molecular aspects of hepatocyte function in primary culture, Xenobiotica 18 (1988) 773–783.

[7] E.R. Lee, J. Marshall, C.S. Siegel, C. Jiang, N.S. Yew, M.R. Nichols, J.B. Nietupski, R.J. Ziegler, M.B. Lane, K.X. Wang, N.C. Wan, R.K. Scheule, D.J. Harris, A.E. Smith, S.H. Cheng, Detailed analysis of structures and formulations of cationic lipids for efficient gene transfer to the lung, Hum. Gene Ther. 7 (1996) 1701–1717.

[8] S. Hama, H. Akita, S. Iida, H. Mizuguchi, H. Harashima, Quantitative and mechanism-based investigation of post-nuclear delivery events between adenovirus and lipoplex, Nucleic Acids Res. 35 (2007) 1533–1543.

[9] S. Hama, H. Akita, R. Ito, H. Mizuguchi, T. Hayakawa, H. Harashima, Quantitative comparison of intracellular trafficking and nuclear transcription between adenoviral and lipoplex systems, Mol. Ther. 13 (2006) 786–794.

[10] N.S. Yew, D.M. Wysokenski, K.X. Wang, R.J. Ziegler, J. Marshall, D. McNeilly, M. Cherry, W. Osburn, S.H. Cheng, Optimization of plasmid vectors for high-level expression in lung epithelial cells, Hum. Gene Ther. 8 (1997) 575–584.

[11] C. Oellig, B. Seliger, Gene transfer into brain tumor cell lines: reporter gene expression using various cellular and viral promoters, J. Neurosci. Res. 26 (1990) 390–396.

[12] Z.L. Xu, H. Mizuguchi, A. Ishii-Watabe, E. Uchida, T. Mayumi, T. Hayakawa, Optimization of transcriptional regulatory elements for constructing plasmid vectors, Gene 272 (2001) 149–156.

[13] Z.L. Xu, H. Mizuguchi, A. Ishii-Watabe, E. Uchida, T. Mayumi, T. Hayakawa, Strength evaluation of transcriptional regulatory elements for transgene expression by adenovirus vector, J. Control. Release 81 (2002) 155–163.

[14] B.S. Chapman, R.M. Thayer, K.A. Vincent, N.L. Haigwood, Effect of intron A from human cytomegalovirus (Towne) immediate-early gene on heterologous expression in mammalian cells, Nucleic Acids Res. 19 (1991) 3979–3986.

[15] M.T. Huang, C.M. Gorman, Intervening sequences increase efficiency of RNA 3′ processing and accumulation of cytoplasmic RNA, Nucleic Acids Res. 18 (1990) 937–947.

[16] P.O. Seglen, Preparation of isolated rat liver cells, Methods Cell Biol. 13 (1976) 29–83.

[17] H. Mizuguchi, M.A. Kay, Efficient construction of a recombinant adenovirus vector by an improved in vitro ligation method, Hum. Gene Ther. 9 (1998) 2577–2583.

[18] K. Kawabata, F. Sakurai, T. Yamaguchi, T. Hayakawa, H. Mizuguchi, Efficient gene transfer into mouse embryonic stem cells with adenovirus vectors, Mol. Ther. 12 (2005) 547–554.

[19] H. Mizuguchi, M.A. Kay, A simple method for constructing E1- and E1/E4-deleted recombinant adenoviral vectors, Hum. Gene Ther. 10 (1999) 2013–2017.

[20] H. Niwa, K. Yamamura, J. Miyazaki, Efficient selection for high-expression transfectants with a novel eukaryotic vector, Gene 108 (1991) 193–199.

[21] J.V. Maizel Jr., D.O. White, M.D. Scharff, The polypeptides of adenovirus. I. Evidence for multiple protein components in the virion and a comparison of types 2, 7A, and 12, Virology 36 (1968) 115–125.

[22] J.M. Bergelson, J.A. Cunningham, G. Droguett, E.A. Kurt-Jones, A. Krithivas, J.S. Hong, M.S. Horwitz, R.L. Crowell, R.W. Finberg,

Isolation of a common receptor for coxsackie B viruses and adenoviruses 2 and 5, Science 275 (1997) 1320–1323.
[23] L.J. Henry, D. Xia, M.E. Wilke, J. Deisenhofer, R.D. Gerard, Characterization of the knob domain of the adenovirus type 5 fiber protein expressed in *Escherichia coli*, J. Virol. 68 (1994) 5239–5246.
[24] M. Bai, B. Harfe, P. Freimuth, Mutations that alter an Arg-Gly-Asp (RGD) sequence in the adenovirus type 2 penton base protein abolish its cell-rounding activity and delay virus reproduction in flat cells, J. Virol. 67 (1993) 5198–5205.
[25] T.J. Wickham, P. Mathias, D.A. Cheresh, G.R. Nemerow, Integrins alpha v beta 3 and alpha v beta 5 promote adenovirus internalization but not virus attachment, Cell 73 (1993) 309–319.
[26] N. Koizumi, H. Mizuguchi, F. Sakurai, T. Yamaguchi, Y. Watanabe, T. Hayakawa, Reduction of natural adenovirus tropism to mouse liver by fiber-shaft exchange in combination with both CAR- and alphav integrin-binding ablation, J. Virol. 77 (2003) 13062–13072.
[27] N. Koizumi, K. Kawabata, F. Sakurai, Y. Watanabe, T. Hayakawa, H. Mizuguchi, Modified adenoviral vectors ablated for coxsackievirus–adenovirus receptor, alphav integrin, and heparan sulfate binding reduce in vivo tissue transduction and toxicity, Hum. Gene Ther. 17 (2006) 264–279.
[28] F. Sakurai, H. Mizuguchi, T. Yamaguchi, T. Hayakawa, Characterization of in vitro and in vivo gene transfer properties of adenovirus serotype 35 vector, Mol. Ther. 8 (2003) 813–821.
[29] M. Gossen, S. Freundlieb, G. Bender, G. Muller, W. Hillen, H. Bujard, Transcriptional activation by tetracyclines in mammalian cells, Science 268 (1995) 1766–1769.
[30] F. Yao, T. Svensjo, T. Winkler, M. Lu, C. Eriksson, E. Eriksson, Tetracycline repressor, tetR, rather than the tetR-mammalian cell transcription factor fusion derivatives, regulates inducible gene expression in mammalian cells, Hum. Gene Ther. 9 (1998) 1939–1950.
[31] K.S. Christopherson, M.R. Mark, V. Bajaj, P.J. Godowski, Ecdysteroid-dependent regulation of genes in mammalian cells by a *Drosophila* ecdysone receptor and chimeric transactivators, Proc. Natl. Acad. Sci. USA 89 (1992) 6314–6318.
[32] Y. Wang, B.W. O'Malley Jr., S.Y. Tsai, B.W. O'Malley, A regulatory system for use in gene transfer, Proc. Natl. Acad. Sci. USA 91 (1994) 8180–8184.
[33] Z.L. Xu, H. Mizuguchi, T. Mayumi, T. Hayakawa, Regulated gene expression from adenovirus vectors: a systematic comparison of various inducible systems, Gene 309 (2003) 145–151.

Differentiation (2008) 76:495–505 DOI: 10.1111/j.1432-0436.2007.00245.x

ORIGINAL ARTICLE

Etsuko Ikeda · Kiyohito Yagi · Midori Kojima · Takahiro Yagyuu · Akira Ohshima · Satoshi Sobajima · Mika Tadokoro · Yoshihiro Katsube · Katsuhiro Isoda · Masuo Kondoh · Masaya Kawase · Masahiro J Go · Hisashi Adachi · Yukiharu Yokota · Tadaaki Kirita · Hajime Ohgushi

Multipotent cells from the human third molar: feasibility of cell-based therapy for liver disease

Received June 4, 2007; accepted in revised form September 17, 2007

Abstract Adult stem cells have been reported to exist in various tissues. The isolation of high-quality human stem cells that can be used for regeneration of fatal deseases from accessible resources is an important advance in stem cell research. In the present study, we identified a novel stem cell, which we named tooth germ progenitor cells (TGPCs), from discarded third molar, commonly called as wisdom teeth. We demonstrated the characterization and distinctiveness of the TGPCs, and found that TGPCs showed high proliferation activity and capability to differentiate *in vitro* into cells of three germ layers including osteoblasts, neural cells, and hepatocytes. TGPCs were examined by the transplantation into a carbon tetrachloride (CCl_4)-treated liver injured rat to determine whether this novel cell source might be useful for cell-based therapy to treat liver diseases. The successful engraftment of the TGPCs was demonstrated by PKH26 fluorescence in the recipient's rat as to liver at 4 weeks after transplantation. The TGPCs prevented the progression of liver fibrosis in the liver of CCl_4-treated rats and contributed to the restoration of liver function, as assessed by the measurement of hepatic serum markers aspartate aminotransferase and alanine aminotransferase. Furthermore, the liver functions, observed by the levels of serum bilirubin and albumin, appeared to be improved following transplantation of TGPCs. These findings suggest that multipotent TGPCs are one of the candidates for cell-based therapy to treat liver diseases and offer unprecedented opportunities for developing therapies in treating tissue repair and regeneration.

Key words tooth germ · multipotent · hepatocyte · transplantation

Etsuko Ikeda[1] (✉) · Akira Ohshima · Satoshi Sobajima · Mika Tadokoro · Yoshihiro Katsube · Masahiro J Go · Hisashi Adachi · Yukiharu Yokota · Hajime Ohgushi
Research Institute for Cell Engineering (RICE)
National Institute of Advanced Industrial Science and Technology (AIST)
3-11-46 Nakoji, Amagasaki
Hyogo 661-0974, Japan
Tel: +81 6 6494 7807
Fax: +81 6 6494 7861
E-mail: etu-ikeda@aist.go.jp

Kiyohito Yagi[1] · Midori Kojima · Katsuhiro Isoda · Masuo Kondoh · Masaya Kawase
Graduate School of Pharmaceutical Sciences
Osaka University, Suita
Osaka 565-0871, Japan

Takahiro Yagyuu · Tadaaki Kirita
Department of Oral and Maxillofacial Surgery
Nara Medical University, Kashihara
Nara 634-8521, Japan

[1]Both authors are first authors.

Introduction

The incidence of hepatocellular carcinoma (HCC) related to hepatitis C and B continues to increase in developed countries (El-Serag et al., 2003). Chronic liver injury, including that caused by virus infection, causes persistent inflammation and fibrosis, followed by the development of liver cirrhosis and HCC. Thus, the suppression of liver inflammation and/or intra-hepatic fibrogenesis could circumvent the progression to HCC.

The administration of an antiviral agent, such as interferon, can be expected to eradicate the hepatitis virus from infected patients. However, the resulting liver fibrosis is difficult to manage with drug therapy alone. Therefore, the development of an effective treatment for liver fibrosis is urgently needed for treating patients infected with hepatitis.

Recently, stem cell-based therapy has received attention as a possible alternative to organ transplantation, owing to the ability of stem cells to repopulate and differentiate at the engrafted site. Human stem cells, including embryonic stem cells (ES cells) and adult stem cells, are excellent candidates for cell-based therapy, as they can produce differentiated cells and are self-renewing. Furthermore, the enormous ability of human ES cells to differentiate into many cell types of three germ layers is encouraging (Thomson et al., 1998; Reubinoff et al., 2000). However, ethical issues and safety considerations are obstacles to clinical applications. The use of adult stem cells may circumvent the difficulties posed by ES cells, and they hold considerable clinical promise. The source of novel primitive cells that express ES cell markers such as Oct-4 and Nanog (Boyer et al., 2005) and demonstrate a perfect therapeutic effect in animal models with fatal diseases has long been awaited.

Bone marrow stem cells, including pluripotent hematopoietic stem cells (HSCs) and mesenchymal stem cells (MSCs), are thought to have great potential for cell-based therapy (Ohgushi and Caplan, 1999; Ohgushi et al., 2005). Indeed, previous studies demonstrated that bone marrow-derived MSCs can transdifferentiate into hepatocytes in rats (Petersen et al., 1999), mice (Theise et al., 2000a), and humans (Theise et al., 2000b). However, the potential plasticity of these adult stem cells remains to be clearly delineated, because many conflicting and controversial results have been reported.

Adult stem cells can be obtained from various tissues, including dental tissues (Lee et al., 2000; Toma et al., 2001; Zuk et al., 2002; Miura et al., 2003; Kogler et al., 2004; Seo et al., 2004; Yen et al., 2005). We recently showed that dental mesenchymal (dental papilla or pulp) cells from an impacted third molar germ (Fig. 1) are capable of osteogenic differentiation (Ikeda et al., 2006). Because our previous study showed the potential of exploiting the osteogenic differentiation of dental mesenchymal (dental papilla or pulp) cells in bone tissue engineering, we have further investigated the biological properties of these mesenchymal cells. We also investigated whether this possible novel source of adult stem cells might be useful for cell-based strategies to treat fatal diseases, such as liver cirrhosis and HCC. To explore the characteristics of these mesenchymal cells, we identified and characterized the clonal cell populations of dental mesenchymal (dental papilla or pulp) cells, which we call tooth germ progenitor cells (TGPCs). To investigate whether TGPCs might be useful for the treatment of liver damage, we then examined the ability of the human TGPCs to differentiate into hepatocytes and their potential effectiveness in suppressing liver inflammation and preventing liver fibrosis in carbon tetrachloride (CCl_4)-treated rats.

Materials and methods

Harvest of dental mesenchyme

This study was approved by the ethics committee of the National Institute of Advanced Industrial Science and Technology (AIST). Partially mineralized and impacted third molar tooth germs with no eruption into the oral cavity were collected from five individuals aged 10–13 years under local anesthesia, and with written informed consent obtained from each individual and the parents of each subject. We used the dental mesenchyme of the third molar tooth germs at the late bell stage (Figs. 1C,1F,1G), one of the four stages of tooth development shown in Figure 1. The third molars were removed by raising soft tissue flaps for adequate exposure and removing the alveolar crest bone with high-speed surgical burrs. The dental mesenchyme (dental papilla or pulp, approximately 0.4 g, Fig. 1H) was separated from the dental follicle (Fig. 1G) in the extracted third molar using forceps.

Isolation and expansion of TGPCs

The dental mesenchyme was finely minced, digested with 10 ml of 4 mg/ml collagenase (Wako, Osaka, Japan) in phosphate-buffered saline (PBS) supplemented with 1 mM $CaCl_2$, and shaken at 37°C for 30 min. The samples were then centrifuged at 400 × *g* for 10 min at 4°C to obtain a pellet, which was then suspended in maintenance medium (10 ml): Eagle's α minimal essential medium (α-MEM; Invitrogen Co., Carlsbad, CA) containing 10% fetal bovine serum (FBS; JRH Biosciences; Lenexa, KS) and the same antibiotic mixture as described previously (Ikeda et al., 2006). The cell suspension (10 ml) was placed in a 10-cm dish in the maintenance medium for primary culture. The medium was changed twice a week. During culture, cell debris and floating cells were removed, resulting in the proliferation of adherent fibroblastic cells.

At approximately 1 week, the cells became nearly confluent and were trypsinized with 0.05% trypsin and 0.53 mM EDTA. They were then seeded directly into 96-well plates at a one-cell-per-well density using the Clonecyte system of flow cytometry (FACS) Vantage (Becton Dickinson, Franklin Lakes, NJ) (passage 1). To select wells containing a single cell, the number of cells in each well was counted three times independently by different researchers. Only one cell was found in most wells, and the average colony-forming efficiency of the single cells was approximately 70%. The clonal expansion efficiency was high for all the dental mesenchyme from all five individuals. A preliminary study showed that approximately 30% of the clonal cells had *in vitro* osteogenic differentiation capability. Several growing colonies with a high proliferative activity were selected after several passages. The clonally expanded cells were trypsinized and divided into three wells of six-well plates (passage 2) for expansion. For further expansion, the cells were trypsinized and seeded at 1×10^5 cells/flask in a T-75 Flask (passage 3). They were then trypsinized and suspended at a concentration of 1×10^6 cells/ml in a Cell Banker (Juji Field, Tokyo, Japan) for cryopreservation at −80°C (passage 4). The cells were later thawed and seeded at 1×10^5 cells/flask in a T-75 Flask for expansion. TGPCs were harvested after 7 days (passage 5) and used for differentiation assays or cell-surface analyses.

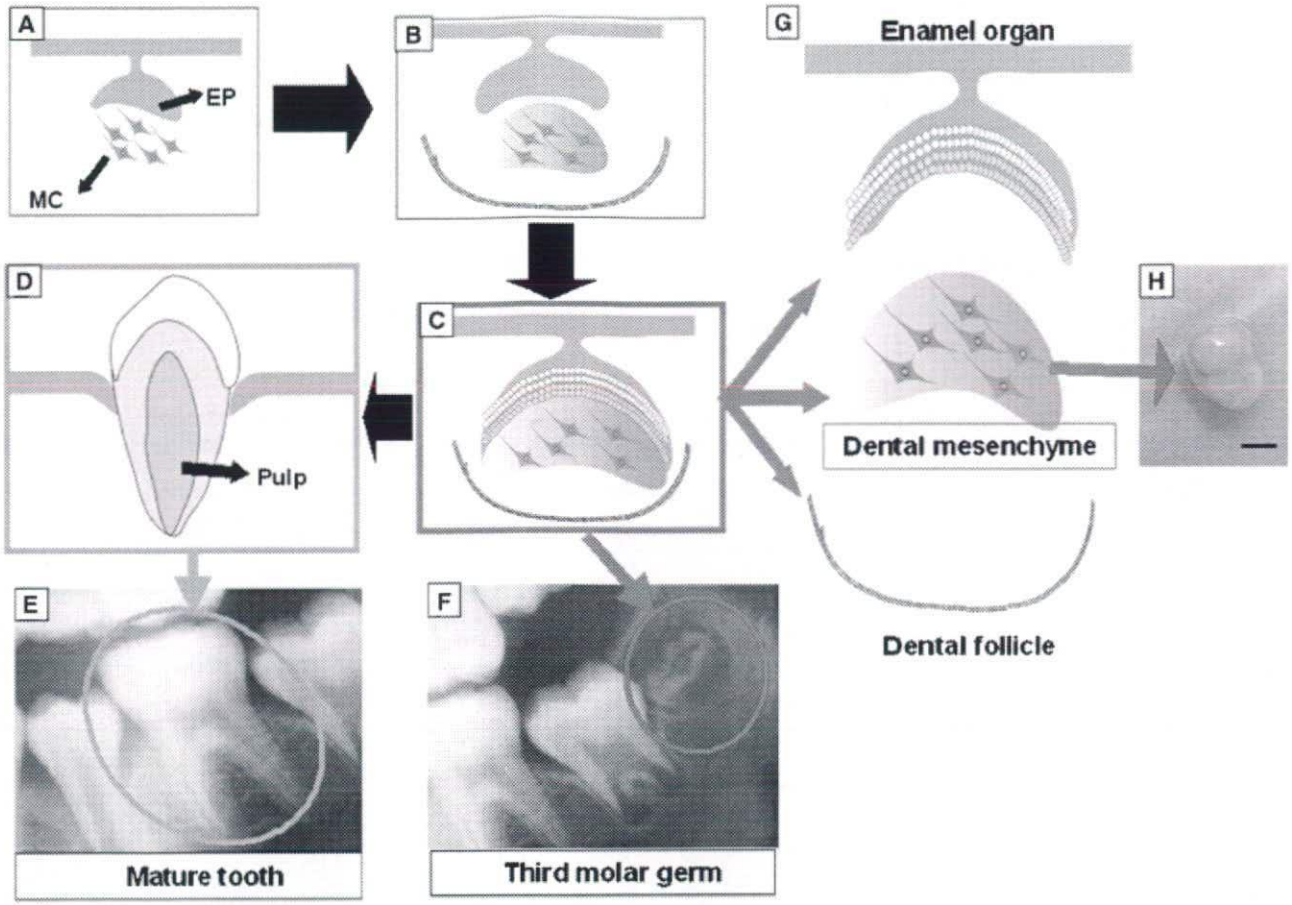

Fig. 1 Tooth development and dental mesenchyme. Bud stage; growth of epithelial cells (EP) and proliferation of mesenchymal cells (MC) (**A**). Cap stage; the epithelial bud enlarges into a rounded structure. MC gather and form dental mesenchyme (**B**). Bell stage, differentiation and calcification occur in the late bell stage. In this stage, the tooth germ consists of all three components (enamel organ, dental mesenchyme [dental pulp or papilla], and dental follicle) (**C**). Tooth maturation, a mature tooth including pulp (**D**). Radiography of a mature tooth (**E**). Radiography of the tooth germ of third molar in the mandibular bone (**F**). Three parts of tooth germ in the late bell stage (**G**). Dental mesenchyme (dental pulp or papilla, **H**). Scale bar = 5 mm.

Preparation of TGPCs with a variant of green fluorescent protein (Venus)

For observation of TGPCs with a stable expression of Venus, a variant of GFP, we utilized a murine stem cell virus (MSCV) retroviral expression system (BD Biosciences Clontech, Palo Alto, CA). The Venus gene was generously provided by Dr. A. Miyawaki (Nagai et al., 2002). We preparated a retroviral vector pMSCV encoding Venus (Venus/pMSCV) by sub-cloning of the Venus cDNA into the pMSCVneo vector. For retroviral production, a PT67 packaging cell line was transfected with the Venus/pMSCV vector using a Fugene 6 transfection reagent (Roche Diagnostics, Basel, Switzerland) according to the manufacturer's instructions. The PT67 cells were passaged the following day in the presence of 400 μg/ml Geneticin (G418, Invitrogen). After further culture for a couple of passages, almost all PT67 cells became positive for fluorescence from the Venus protein.

For infection of TGPCs, the PT67 cells were cultured to obtain virus-containing supernatants, and the supernatant was filtered through a 0.45-μm cellulose acetate filter. The supernatant was then supplemented with 4 μg/ml polybrene for the final concentration (Chemicon Inc., Temecula, CA). Target TGPCs were incubated in the supernatant containing virus/polybrene overnight. The infection experiments were repeated twice at a 1-day interval. On the day following the second infection, G418 was added for a final concentration of 400 μg/ml for selection. The cells were passaged twice, and Venus-transfected TGPCs were cryopreserved at −80°C. The cryopreserved TGPCs were thawed and used for *in vivo* osteogenic differentiation experiment.

In vitro osteogenic differentiation

TGPCs (passage 5) were seeded at 1×10^4 cells/well in a 12-well plate in maintenance medium. After osteogenic induction was conducted, the alkaline phosphatase (ALP) activity assay, assessment of osteocalcin content, and ALP and alizarin red S stainings were performed as described in our previous studies (Ikeda et al., 2006).

In vivo osteogenic differentiation

TGPCs (passage 5) or TGPCs transfected with Venus, (passage 6) were suspended at 1×10^6 cells/ml in the maintenance medium. Hydroxyapatite (HA) ceramic disks (CELLYARD™; Pentax Co., Tokyo, Japan; 5 mm in diameter; 2 mm thick; pores 100 μm in diameter; an average void volume of 50%) were soaked in the TGPCs suspension at 37°C for 24 hr, and then cultured for 2 weeks under osteogenic induction to make a composite of HA with TGPCs or with TGPCs transfected with Venus as described previously (Ikeda

Table 1 Primers for reverse transcription-polymerase chain reaction

Gene	Primer sequence
Oct-4	
Forward	5′-CGACCATCTGCCGCTTTGAG-3′
Reverse	5′-CCCCCTGTCCCCCATTCCT-3′
Nanog	
Forward	5′-TGCCTCACACGGAGACTGTC-3′
Reverse	5′-TGCTATTCTTCGGCCAGTTG-3′
β-actin	
Forward	5′-CCTTCCTGGGCATGGAGTC-3′
Reverse	5′-CACATCTGCTGGAAGGTGGA-3′
AFP	
Forward	5′-CTCGTTGCTTACACAAAGAAAG-3′
Reverse	5′-ATGGAAAATGAACTTGTCATCA-3′
Albumin	
Forward	5′-TGCTTGAATGTGCTGATGACAGG-3′
Reverse	5′-AAGGCAAGTCAGCAGGCATCTCA-3′
CK18	
Forward	5′-GAGATCGAGGCTCTCAAGGA-3′
Reverse	5′-CAAGCTGGCCTTCAGATTTC-3′
CK19	
Forward	5′-ATGGCCGAGCAGAACCGGAA-3′
Reverse	5′-CCATGAGCCGCTGGTACTCC-3′
Nestin	
Forward	5′-CAGCGTTGGAACAGAGGTTGG-3′
Reverse	5′-TGGCACAGGTGTCTCAAGGGTAG-3′
Tuj-1	
Forward	5′-AGATGTACGAAGACGACGAGGAG-3′
Reverse	5′-GTATCCCCGAAAATATAAACACAA-3′
Neurofilament	
Forward	5′-TGGGAAATGGCTCGTCATTT-3′
Reverse	5′-CTTCATGGAAGCGGCCAATT-3′
Human alu	
Forward	5′-CGAGGCGGGTGGATCATGAGGT-3′
Reverse	5′-TCTGTCGCCCAGGCCGGACT-3′
Rat GAPDH	
Forward	5′-ATGCTGGTGCTGAGTATGTCG-3′
Reverse	5′-GTGGTGCAGGATGCATTGCTGA-3′

AFP, α-fetoprotein; CK18, cytokeratin18; CK19, cytokeratin19; Tuj-1, Class III β-tubulin.

et al., 2006). The composites were implanted subcutaneously in five immunocompromised animals (7-week-old male Fischer 344 rats; NJcl-rnu). The animals were sacrificed 6 weeks after implantation, and the implants with TGPCs or Venus-transfected TGPCs were harvested, fixed in 10% buffered formalin, decalcified with a chelating agent K-CX solution (Falma Co., Tokyo, Japan), and embedded in paraffin. The embedded samples were cut into sections parallel to the round surface, and stained with hematoxylin & eosin (HE). The implants with Venus-transfected TGPCs were immersed in hexane chilled in dry ice. The TGPCs-derived cells were observed with a fluorescence microscope for bone formation.

In vitro neural differentiation

TGPCs (passage 5) were seeded at 2.5×10^3 cells/well in a 12-well culture plate and cultured in α-MEM supplemented with 1% FBS, the antibiotic mixture, 50 ng/ml epidermal growth factor (EGF, PeproTech; London, UK), and 50 ng/ml platelet-derived growth factor (PDGF)-BB (R&D Systems Inc., Minneapolis, MN) for 3 days. Subsequently, the cells were cultured in α-MEM with 1% FBS, the antibiotic mixture, and 50 ng/ml basic fibroblast growth factor (bFGF, PeproTech) for 11 days, for neural differentiation.

In vitro hepatic differentiation

TGPCs (passage 5) were seeded at 5×10^3 cells/well in a collagen-coated six-well culture plate (Nitta Gelatin Inc., Osaka, Japan) for hepatic induction, which required three steps. For hepatic specification (step 1), the cells were cultured in low-glucose Dulbecco's minimal essential medium (DMEM, GIBCO, NY, USA) supplemented with 2% FBS, the antibiotic mixture, 2 mM L-glutamine (Nacalai Tesque, Kyoto, Japan), and 100 ng/ml acidic fibroblast growth factor (a-FGF, PeproTech) for 5 days. For hepatic commitment (step 2), the cells were cultured in low-glucose DMEM with 2% FBS, the antibiotic mixture, 2 mM L-glutamine, and 20 ng/ml hepatocyte growth factor (HGF, R&D Systems Inc.) for 5 days. Finally, for hepatic differentiation (step 3), the cells were cultured in low-glucose DMEM with 2% FBS, the antibiotic mixture, 2 mM L-glutamine, 20 ng/ml HGF, 10 nmol/l dexamethasone (Dex, Wako), insulin-transferrin-selenium-X (ITS-X, GIBCO), and 10 ng/ml oncostatin M (OSM, R&D Systems Inc.) for 11 days. The TGPCs were also cultured for 21 days in basal medium containing low-glucose DMEM with 2% FBS, the antibiotic mixture, and 2 mM L-glutamine as the control without hepatic induction.

In vivo hepatic differentiation

TGPCs were or were not induced to differentiate into hepatocyte-like cells (hepatic induction). After the 3-week hepatic induction, TGPCs were stained using the PKH Fluorescent Cell Linker Kit (Sigma Aldrich, St. Louis, MO) as described previously (Oyagi et al., 2006). Immunocompromised Fisher 344 rats aged 9 weeks were given an intra-peritoneal (i.p.) injection of 1 ml/kg CCl_4 in olive oil. Control animals received olive oil i.p. Two days later, 1×10^7 TGPCs were transplanted by injection into the portal vein. Sham-operated rats received a 500 μl PBS injection. The CCl_4 treatment was performed twice a week for 4 weeks at the same dose as the first treatment, and the liver was then excised and immersed in hexane chilled in dry ice. The TGPCs-derived cells were observed with a fluorescence microscope for evidence of engraftment. The liver was harvested, and liver specimens were fixed with 10% buffered formalin and embedded in paraffin. Tissue sections were mounted on slides and stained with Azan, and the extent of fibrosis was analyzed. The fibrotic area was quantified using NIH image software. The percentage of the area showing fibrosis (blue staining) was calculated. HE staining was also performed. The blood was collected from the heart using a 21 G needle, and the serum was frozen and stored at −80°C. Serum aspartate aminotransferase (AST) and alanine aminotransferase (ALT) levels were measured using an assay kit (Transaminase CII-Test Wako, Wako). The total bilirubin and serum albumin levels were determined using an assay kit (Azwell, Osaka, Japan) and an Albumin B Test Kit (Wako), respectively. Hydroxyproline content was determined as described elsewhere (Sakaida et al., 2004).

Cell surface analysis

The cell-surface analysis of TGPCs (passage 5) was performed as described in our previous report. Fluorescein isothiocyanate (FITC)-conjugated antibodies against CD14, CD34, CD44, CD45, CD90, CD105, CD166 (Invitrogen), and CD29 (Serotec, Oxford, UK), and HLA-Class I, HLA-DR (Invitrogen), and STRO-1 (Development Study of Hybridoma Bank, DSHB, IA) were used. Mouse immunoglobulin IgG-FITC (Beckman Coulter Inc., Fullerton, CA) was used as a negative control.

Reverse transcriptase-polymerase chain reaction (RT-PCR)

Total RNA isolation and first-strand cDNA synthesis were conducted as reported previously (Ikeda et al., 2006). DNA was extracted from the liver using a TaKaRa DEXPAT™ kit (TaKaRa

Biomedicals, Kyoto, Japan). A PCR was performed using the GeneAmp PCR System 9700 (Applied Biosystems, Foster City, CA) at 94°C–96°C for 5–12 min, and 25–35 cycles at 94°C for 30 sec, 60°C–74°C for 30 sec, and 72°C for 1 min. The primer pairs used for RT-PCR analysis were designed to amplify fragments of Oct-4, Nanog, albumin, α-fetoprotein (AFP), cytokeratin 18 (CK18), cytokeratin 19 (CK19), nestin, class III β-tubulin (TuJ1), neurofilament, human *alu*, rat glyceraldehyde-3-phosphate dehydrogenase (GAPDH), and β-actin (Table 1).

Immunocytochemistry

The TGPCs were fixed with 4% paraformaldehyde (PFA) for 10 min at room temperature, treated with 0.1% Triton-X 100 (Sigma Aldrich) for 10 min, and incubated sequentially with primary monoclonal antibodies at room temperature for 4 hr. Primary antibodies against the human albumin (Cappel, West Chester, PA), TuJ1 (Covance Inc., Princeton, NJ), and nestin (Chemicon, Los Angeles, CA) were used at a dilution of 1:100. The samples were then rinsed three times with PBS and incubated for 60 min at room temperature with FITC-conjugated secondary antibodies at 1:100. Staining was visualized under an Olympus IX70 fluorescence microscope (Olympus, Tokyo, Japan).

Western blotting

The primary antibody used was against the human albumin antigen (Cappel). Western blotting analysis was carried out as reported previously (Oyagi et al., 2006).

Statistical analysis

Values are expressed as the mean and standard deviation (SD). There were two groups of continuous variables in this study. The data were analyzed for statistical significance using Dunnett's multiple comparison test, Welch's *t*-test, and Student's *t*-test. p-values <0.05 were considered to be statistically significant.

Results

Isolation and characterization of TGPCs

We successfully established the methods to obtain primary cultured cells from the tooth germ (Fig. 1C), which is often eliminated during the extraction of the third molar (third molar germ, Fig. 1F) at an immature stage of tooth development. Tooth development occurs from the neural crest and goes through four morphological stages including bud (Fig. 1A), cap (Fig. 1B), bell (Fig. 1C), and final maturation (Figs. 1D,1E). In this study, we used dental mesenchyme of the tooth germ in the late bell stage (Figs.1C,1F,1G). After expansion of primary cultured cells from dental mesenchyme tissue (Fig. 1H), the deposition of single sorted cells into individual wells of 96-well plates was performed to obtain a stable and robust clonal cell line. The culture-expanded cells were tested for growth potential, and several single-cell-derived clones were selected among the clones grown. The clonal cells, TGPCs, were selected based on the exhibition of comparable growth characteristics, as shown in Figure 2A. TGPCs were expanded and maintained for nearly 60 population doublings, during which they retained their morphology, i.e., small spindle-shaped cells with a reduced cytoplasm (Fig. 2B). Interestingly, RT-PCR analysis showed that the TGPCs expressed two transcription factors for pluripotency: Oct-4 and Nanog (Fig. 2C). These observations indicated that TGPCs have novel primitive stem cell properties because these transcription factors are involved in the regulation of cell growth and differentiation and normally restricted to pluripotent cells of the developing embryo such as epiblast cells and primordial germ cells (Boyer et al., 2005). The analysis of the cell surface by FACS demonstrated that the TGPCs were defined by expression of the following markers: CD29, CD44, CD90, CD105, CD166, and HLA-Class I. For STRO-1, TGPCs expressed at a low level. In addition, they were negative for CD14, CD34, CD45, and HLA-DR (Fig. 2D). Expression of this marker pattern was consistent in all TGPCs regardless of the donor's age or gender. The pattern of cell surface antigen expression did not vary in several TGPCs clones. Thus, the TGPCs were negative for hematopoietic markers (CD14, CD34, and CD45) but strongly positive for markers present in mesenchymal cells (CD29, CD44, CD90, CD105, and CD166) and weakly positive for STRO-1, indicating that TGPCs have a mesenchymal phenotype.

Osteogenic and neural differentiation capabilities of TGPCs

We evaluated the osteogenic differentiation potential of TGPCs cultured in the presence or in the absence of Dex. Both the ALP activity and bone-specific osteocalcin content in TGPCs with Dex (Dex+) were significantly higher than in those cultured without Dex (Dex−, Figs. 3A,3B). In addition, TGPCs cultured with Dex stained strongly with the ALP and Alizarin red S, indicating that they had the mineralizing capability of differentiated osteoblasts (Figs. 3C,3D).

Furthermore, we investigated the osteogenic differentiation potential of TGPCs *in vivo*. TGPCs were combined with HA ceramic disks and cultured to make a composite of HA with TGPCs or with TGPCs transfected with Venus, a variant of GFP. The composites were then subcutaneously implanted in immunocompromised rats. Histological sections of the HA/TGPCs implants depicted new bone formation in the pore area of the HA. Bone formation was indicated by the presence of osteocytes in the newly formed bone matrix, together with a cuboidal-shaped active osteoblast lining on the matrix surface (Fig. 3E). The analysis of the implants with Venus-transfected TGPCs showed that Venus-positive TGPCs were located within the mineralized matrix, in which osteoblasts and osteocytes were typically found (Fig. 3F).

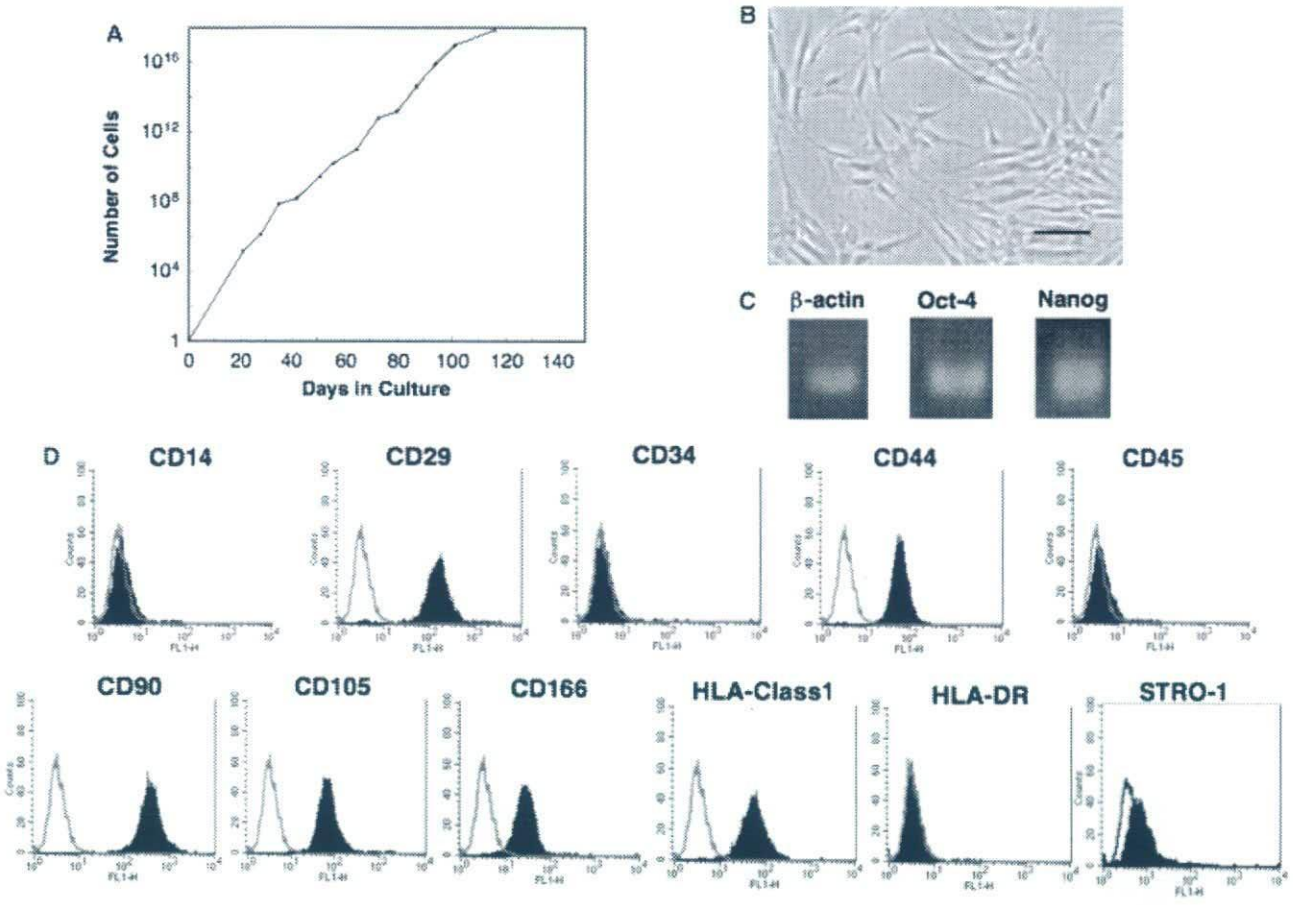

Fig. 2 Characteristics of TGPCs. Expansion in long-term culture (**A**). Morphology at passage 5. A homogeneous population of small spindle-shaped cells was seen (**B**). Scale bar = 100 μm. RT-PCR analysis for Oct-4, and Nanog (β-actin as a control, **C**). Cell surface analysis. Negative for CD14, CD34, CD45, and HLA-DR. Positive for CD29, CD44, CD90, CD105, CD166, HLA-Class I, and STRO-1. Open and closed histograms stand for control immunoglobulin and specific antibody, respectively (**D**). TGPC, tooth germ progenitor cells; RT-PCR, reverse transcriptase-polymerase chain reaction.

To assess neural differentiation potential, neural-induced TGPCs were cultured. By 7 days after the start of neural induction, some of the cells had a neuron-like bipolar-spindle morphology. By day 14, these cells stained positive for nestin and neuron-specific TuJ1 (Figs. 3G,3H). The expression of neural-specific marker genes such as nestin, TuJ1, and neurofilament was observed by RT-PCR at different time points (Fig. 3I). After induction of neural differentiation, the mRNA expression for nestin, TuJ1, and neurofilament gradually increased with time. The results indicate that TGPCs have the potential for neural differentiation *in vitro*.

In vitro hepatic differentiation capability of TGPCs

Next, the hepatic-induced TGPCs were cultured and RT-PCR analysis was performed at different time points (Fig. 4A). RNAs for the liver-specific albumin gene, and for AFP, CK18, and CK19 were expressed to a greater or a lesser extent during the culture period. A weak albumin mRNA signal was detected on day 10, and obvious expression was observed on days 14 and 21. In contrast, starting on day 14, the AFP and CK19 mRNA expressions gradually declined. These results indicated a certain degree of differentiation toward the phenotype of mature hepatocytes, because AFP and CK19 are typical markers of immature hepatocytes and specific biliary epithelial cells, respectively.

Albumin protein analysis was also performed at each time by Western blotting analysis (Fig. 4B), and the results were consistent with those of serial mRNA analysis of albumin. Furthermore, immunocytochemical staining for albumin at day 21 showed that hepatic-induced TGPCs were strongly positive compared with the control (non-induced) TGPCs.

These findings were consistent with the morphological changes that we observed apparently over time (Fig. 4C). The change from a bipolar-spindle and fibroblast-like to a polygonal and an epithelial-like morphology occurred in

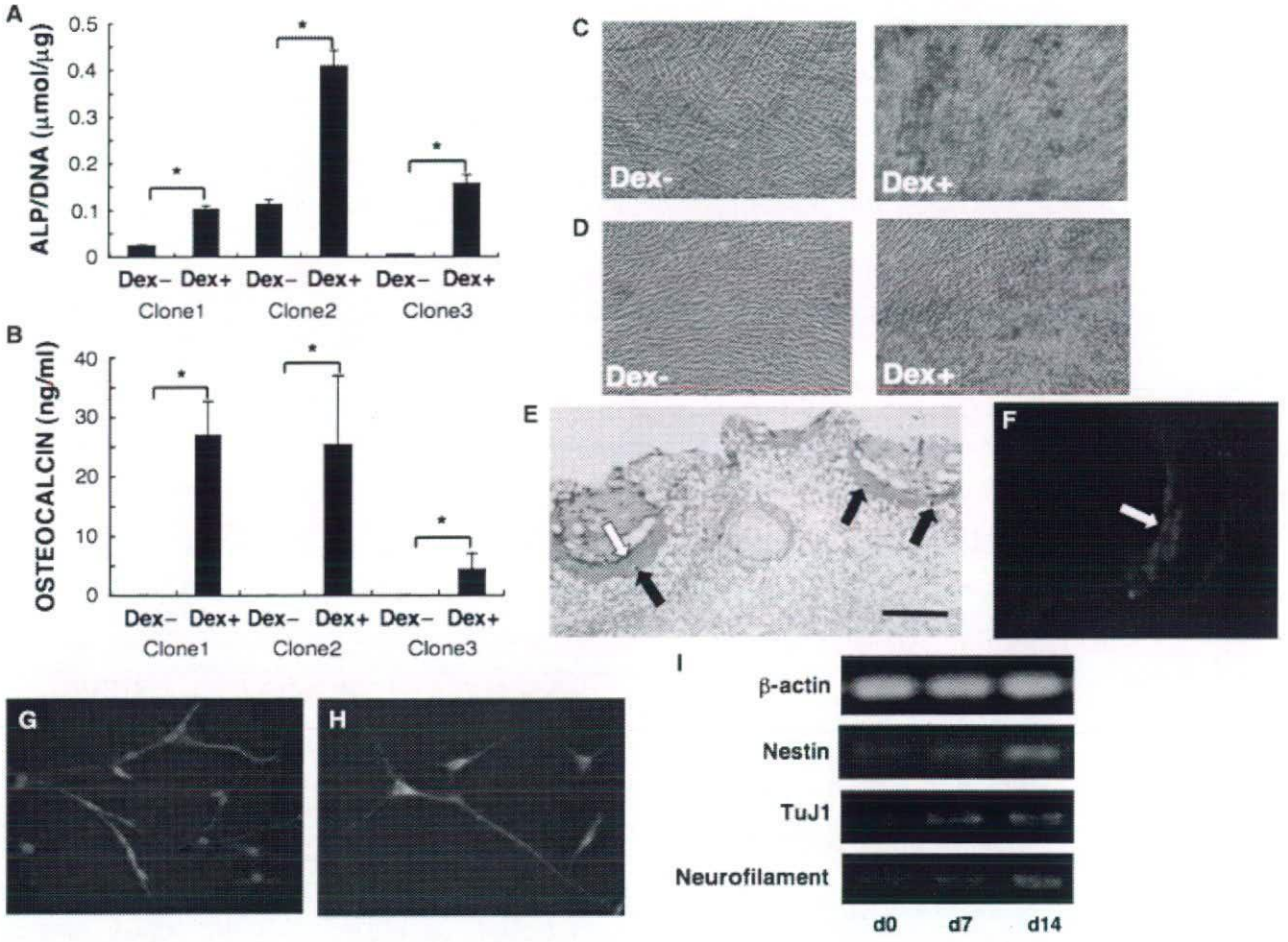

Fig. 3 Osteoblastic and neural differentiation. The ALP activity per microgram of DNA was greater in TGPCs grown with Dex (Dex+) than in those grown without Dex (Dex−) with $n = 5$ per clone. $^*p < 0.05$ (**A**). Osteocalcin content was significantly higher in Dex+than in Dex−cultures ($n = 5$ per clone). $^*p < 0.05$ (**B**). ALP staining: strong ALP staining (red areas) was seen in Dex+cultures (**C**). Alizarin red S staining: obvious calcium mineral deposit (red color) was seen in Dex+cultures (**D**). Histological sections of HA/TGPCs composites at 8 weeks after implantation; new bone formation with osteocytes and osteoblasts was seen in the pore area of the HA. Open and black arrows represent osteoblasts and osteocytes, respectively. (HE staining, scale bar = 100 μm, **E**). Analysis of implants with Venus-transfected TGPCs; Venus gene was expressed in area of new bone formation with osteocytes and osteoblasts (**F**). Immunocytochemical staining for nestin (**G**) and TuJ1 (**H**) in TGPCs cultured for neural induction. Neuron-like cells were observed on day 14. Bipolar-spindle-shaped cells were stained positive for nestin (G) and TuJ1 (H). Cell nuclei were stained with DAPI (G, H). Time course of RT-PCR analysis of neural markers in TGPCs 0, 7, and 14 days after neural induction (**I**). TGPC, tooth germ progenitor cells; RT-PCR, reverse transcriptase-polymerase chain reaction; ALP, alkaline phosphatase; HA, hydroxyapatite; HE, hematoxylin & eosin.

the TGPCs in a manner similar to the C3A cell (human-derived hepatoma cell line), a positive control. These results indicated that TGPCs can differentiate *in vitro* into cells with morphological, phenotypic, and functional characteristics of hepatocytes.

TGPCs engraftment into rats with liver injury

Given the above-mentioned findings, we investigated whether TGPCs could be useful therapeutically for the treatment of liver diseases by cell transplantation. Cultured TGPCs were transplanted *via* the portal vein into the liver of CCl_4-treated rats. The cryostat sections were prepared to confirm the presence of transplanted TGPCs in the liver by PKH26-derived fluorescence images. As shown in Figures 5A,5B, fluorescence was observed in the liver with transplanted TGPCs. Because the stained cells formed a cluster seen in the dotted areas in the section, the transplanted TGPCs appeared to proliferate after engraftment in the liver. We further attempted to detect the human DNA-specific *alu* sequence by PCR to confirm the presence of the donor TGPCs in the rat liver (Fig. 5E). There were no amplified bands for *alu* in the DNA of sham-operated rat liver. In contrast, the bands for *alu* were seen in that of a TGPCs-transplanted rat liver.

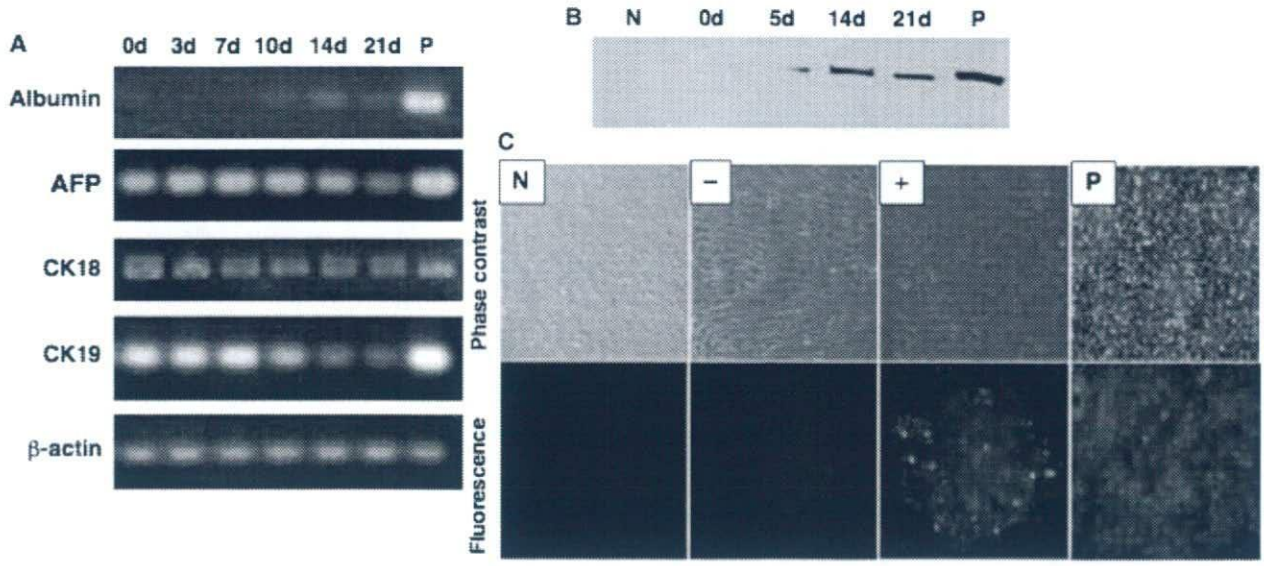

Fig. 4 *In vitro* hepatic differentiation. Time course of reverse transcriptase-polymerase chain reaction analysis of hepatic markers in TGPCs 0, 3, 7, 10, 14, and 21 days after the start of hepatic induction (**A**). Time course of albumin protein expression in TGPCs 0, 5, 14, and 21 days after the start of hepatic induction, by western blotting analysis (**B**). Immunocytochemical staining for albumin. TGPCs cultured for hepatic induction stained positively for albumin, compared with those that were not induced to differentiate. TGPCs with (+) and without (−) hepatic induction (**C**). P indicates the positive control (C3A) and N indicates the negative control (fibroblasts). TGPC, tooth germ progenitor cells.

Regeneration of injured liver in rats that received transplanted TGPCs

Azan (Figs. 6A–6D) and HE (Figs. 6E–6H) stainings were performed to examine the effect of TGPCs transplantation on liver fibrosis. Following staining with Azan, a large area of fibrosis was stained blue and scattered white spots that indicated steatonecrosis were seen in the liver sections of sham-operated rats (Fig. 6B). The extents of fibrosis and steatonecrosis in the liver of CCl_4-treated rats that received transplanted TGPCs that had undergone no hepatic induction (Fig. 6C) were comparable with those in the liver of sham-operated rats (Fig. 6B). In contrast, the transplantation of the differentiated TGPCs suppressed liver fibrosis and steatonecrosis (Fig. 6D). HE staining revealed smaller areas of damage in liver sections from the recipients of hepatic induction-treated TGPCs (Fig. 6H) than in those of sham-operated animals (Fig. 6F). The effect of the TGPCs transplantation on fibrosis was evaluated by digitalization of the area stained blue by Azan (Fig. 6I). We also determined the content of liver hydroxyproline, an index of collagen content, using the method described by Sakaida et al. (2004, Fig. 6J). In agreement with the Azan staining results, the transplantation of the differentiated TGPCs significantly suppressed the hydroxyproline content.

We then used serum hepatic markers to investigate the effect of transplanted TGPCs on liver inflammation. The AST and ALT levels increased markedly to 3,333 and 732 KU, respectively, in the sham-operated rats after the CCl_4 treatment. The serum AST and ALT levels in CCl_4-treated rats that received transplanted TGPCs that had undergone hepatic induction were significantly decreased to 972 and 239 KU, respectively. In contrast, the TGPCs cultured in the basal medium did not affect the levels significantly in CCl_4-treated rats. The serum AST and ALT levels in control animals that received olive oil were 88.9 and 13.5 KU, respectively (Figs. 6K,6L). The serum AST and ALT levels were significantly lower in CCl_4-treated recipients of hepatic induction-treated TGPCs than in sham-operated rats, and the findings indicated that the hepatic differentiation of TGPCs before transplantation into the liver was effective in suppressing liver inflammation.

The serum level of total bilirubin increased, whereas the level of albumin decreased after the CCl_4 treatment in the control rats. The transplantation of the differentiated TGPCs reduced both the increase in bilirubin and the suppression of albumin (Figs. 6M,6N).

Discussion

In this study, we characterized clonally expanded TGPCs in terms of their morphology, proliferation, and multipotency. *In vitro*, TGPCs had a mesenchymal phenotype, were self-renewing, and differentiated into cells of three germ layers. Furthermore, transplanted human TGPCs that had undergone hepatic induction survived, and the recipient CCl_4-treated rats showed less injury to the liver than the control animals, suggesting that TGPCs might have clinical applications.

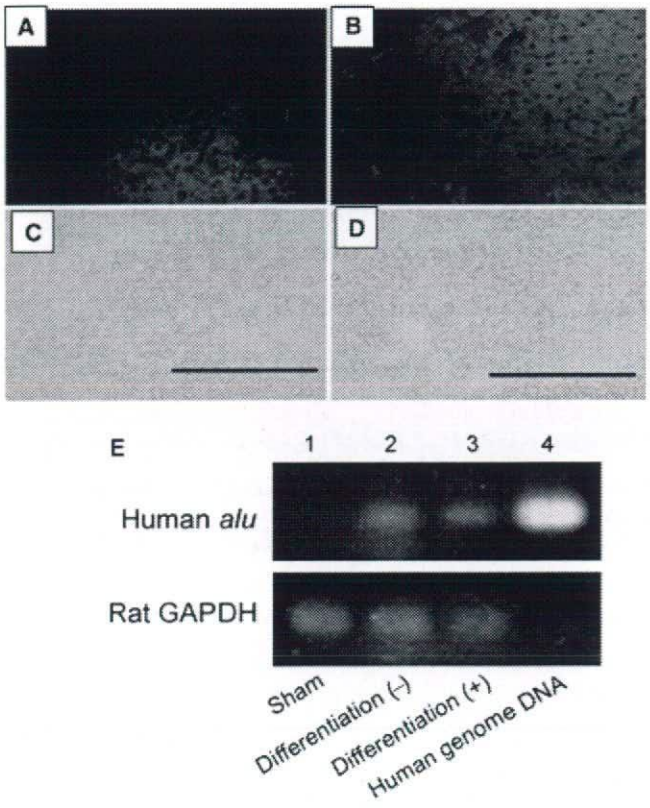

Fig. 5 Transplantation of TGPCs into CCl_4-injured rat liver. Engraftment of TGPCs. Liver sections post transplantation of PKH-26 stained TGPCs cultured without (**A** and **C**) or with (**B** and **D**) hepatic induction. Fluorescence (Upper, A and B) and bright-field (Lower, C and D) images are shown (Scale bars = 100 μm, A–D). Polymerase chain reaction analysis was performed using primers for human alu and rat GAPDH. DNA was isolated from the liver of sham-operated rats (Sham) and of rats after the transplantation of TGPCs with and without hepatic induction (Differentiation (+) and Differentiation (−), respectively). Human genome DNA was the positive control (**E**). TGPC, tooth germ progenitor cells; GAPDH, glyceraldehyde-3-phosphate dehydrogenase; CCl_4, carbon tetrachloride.

Previously, another group showed that clonal cells from the bone marrow differentiate *in vitro* into cells of all three germ layers (Zipori, 2005). Likewise, D'Ippolito et al. (2004) described the same *in vitro* potential for bone marrow-derived adult multilineage inducible (MIAMI) cells. Like MIAMI and other cells that are described in the aforementioned reports (D'Ippolito et al., 2004; Zipori, 2005), TGPCs are thought to be very primitive cells as they showed multilineage differentiation and proliferation capabilities and expressed transcriptional factors associated with pluripotency: Oct-4 and Nanog (Fig. 2).

It has been reported recently that multipotent cells can be isolated from dental tissues such as the dental pulp and dental ligament (Miura et al., 2003; Seo et al., 2004). Iohara et al. (2006) reported that side population cells from porcine dental pulp have the potential for dentinogenesis, chondrogenesis, adipogenesis, and neurogenesis. In these reports, the characterization of clonal cells and the differentiation potential into the endodermal lineage have not been mentioned. Here, this may be the first report that explains the characterization of clonal cells that have greater multipotency than those dental stem cells reported previously and can be obtained from human dental tissues that are discarded during dental treatment. Also, this study provides the first evidence that the stem cells from the neural crest-derived dental tissue can give rise to endoderm cell lineages such as hepatocytes.

Recently, sources of adult stem cells besides the bone marrow, including adipose tissue, term placenta, and placental and/or umbilical cord blood, have been reported. These cells have the potential to differentiate into cell types belonging to tissues besides their tissue of origin (Zuk et al., 2002; Kogler et al., 2004; Yen et al., 2005). For example, and with regard to hepatic differentiation, Seo et al. (2005) reported that human adipose tissue-derived stromal cells transplanted into CCl_4-injured SCID (severe combined immunodeficiency) mice differentiate into hepatocytes *in vivo*. Another recent report demonstrated that umbilical cord blood stem cells differentiate into hepatocytes after transplantation into CCl_4-injured rats (Tang et al., 2006). However, these reports did not address the therapeutic effects of these cells.

We and other groups successfully demonstrated that CCl_4-induced liver fibrosis was suppressed following the transplantation of bone marrow-derived MSCs into rats (Oyagi et al., 2006) and mice (Sakaida et al., 2004). Importantly, in the present study, we succeeded in cloning multipotent adult progenitor cells (TGPCs) from the human tooth germ, and showed that TGPCs that were subjected to *in vitro* hepatic induction had a significant therapeutic effect on CCl_4-induced liver injury (Fig. 4). Following clonal expansion, differentiated TGPCs suppressed inflammation and fibrosis in the liver of CCl_4-treated rats and contributed to the restoration of liver function, as assessed by the measurement of hepatic serum markers (Fig. 6). Thus, the extensive proliferation and differentiation capabilities of TGPCs are promising in terms of them being an accessible source for liver tissue engineering approaches.

Our data showed that novel multipotent progenitor cells, TGPCs, might have greater potential for proliferation than the "gold standard" bone marrow MSCs. Furthermore, taking into account the durable viability of cryopreserved TGPCs, it is possible that such cells could be frozen and used later, as needed, in regenerative medicine for autograft, once the cell banking system has been established. Based on the results of our previous study (Akahane et al., 1999), in which allogeneic MSCs survived *in vivo* with appropriate immunosuppressant treatment, we postulate that allogeneic TGPCs given with immunosuppressants or human leukocyte antigen-matched donor TGPCs may be useful for novel tissue engineering therapies. These

doi:10.1016/j.jmb.2008.11.053 J. Mo

JMB

Available online at www.sciencedirect.com

ScienceDirect

Structure–Function Relationship of Tumor Factor (TNF) and Its Receptor Interaction B Structural Analysis of a Fully Active TNFR1 TNF Mutant

Yohei Mukai[1,2], Hiroko Shibata[2], Teruya Nakamura[3], Yasuo Yoshioka[2,4], Yasuhiro Abe[2], Tetsuya Nomura[1,2] Madoka Taniai[5], Tsunetaka Ohta[5], Shinji Ikemizu[3], Shinsaku Nakagawa[1], Shin-ichi Tsunoda[2], Haruhiko Ka Yuriko Yamagata[3] and Yasuo Tsutsumi[1,2]*

[1]*Graduate School of Pharmaceutical Sciences, Osaka University, 1-6 Yamadaoka, Suita, Osaka 565-0871, Japan*

[2]*Laboratory of Pharmaceutical Proteomics, National Institute of Biomedical Innovation, Osaka 567-0085, Japan*

[3]*Graduate School of Pharmaceutical Sciences, Kumamoto University, Kumamoto 862-0973, Japan*

[4]*The Center for Advanced Research and Education in Drug Discovery and Development, Osaka University, 1-6 Yamadaoka, Suita, Osaka 565-0871, Japan*

[5]*Hayashibara Biochemical Laboratories, Inc., 1-2-3 Shimoishii, Okayama 702-8006, Japan*

Received 9 July 2008; received in revised form 21 November 2008; accepted 22 November 2008
Available online
6 December 2008

Edited by I. Wilson

Tumor necrosis factor (TNF) is an important cy carcinogenesis and excludes infectious pathogens t TNF activates its two receptors [TNF receptor (TN the contribution of each receptor to various host immunologic surveillance is not yet clear. Here, techniques to generate receptor-selective TNF mu one TNFR. These TNF mutants will be useful in th TNFR.

Six amino acids in the receptor binding interface 80, and 140) were randomly mutated by polymer phage libraries comprising over 5 million TNF mu By selecting the mutants without affinity for T successfully isolated 4 TNFR2-selective candidates candidates, respectively. The TNFR1-selective ca mutated near residue 30, whereas TNFR2-selective mutated near residue 140, although both had cor residues 140 and 30, respectively. This finding su display technique was suitable for identifying im TNF interaction with TNFR1 and TNFR2. Purified selective candidate, remained fully bioactive and hac without activating TNFR2, indicating the usefuln mutant in analyzing TNFR1 receptor function.

To further elucidate the receptor selectivity of I structure of R1-6 by X-ray crystallography. The resu and R32G mutations strongly influenced electro TNFR2, and that L29K mutation contributed to t TNFR1. This phage display technique can be used functional mutants for analysis of the TNF structure which might facilitate *in silico* drug design based or

Keywords: TNF; X-ray crystallography; phage displa receptor specificity

**Corresponding author.* Department of Toxicology, Graduate School of Pharmaceutical Science Yamadaoka, Suita, Osaka 565-0871, Japan. E-mail address: ytsutsumi@phs.osaka-u.ac.jp.

Abbreviations used: TNF, tumor necrosis factor; TNFR, TNF receptor; SPR, surface plasmon type TNF; PDB, Protein Data Bank.

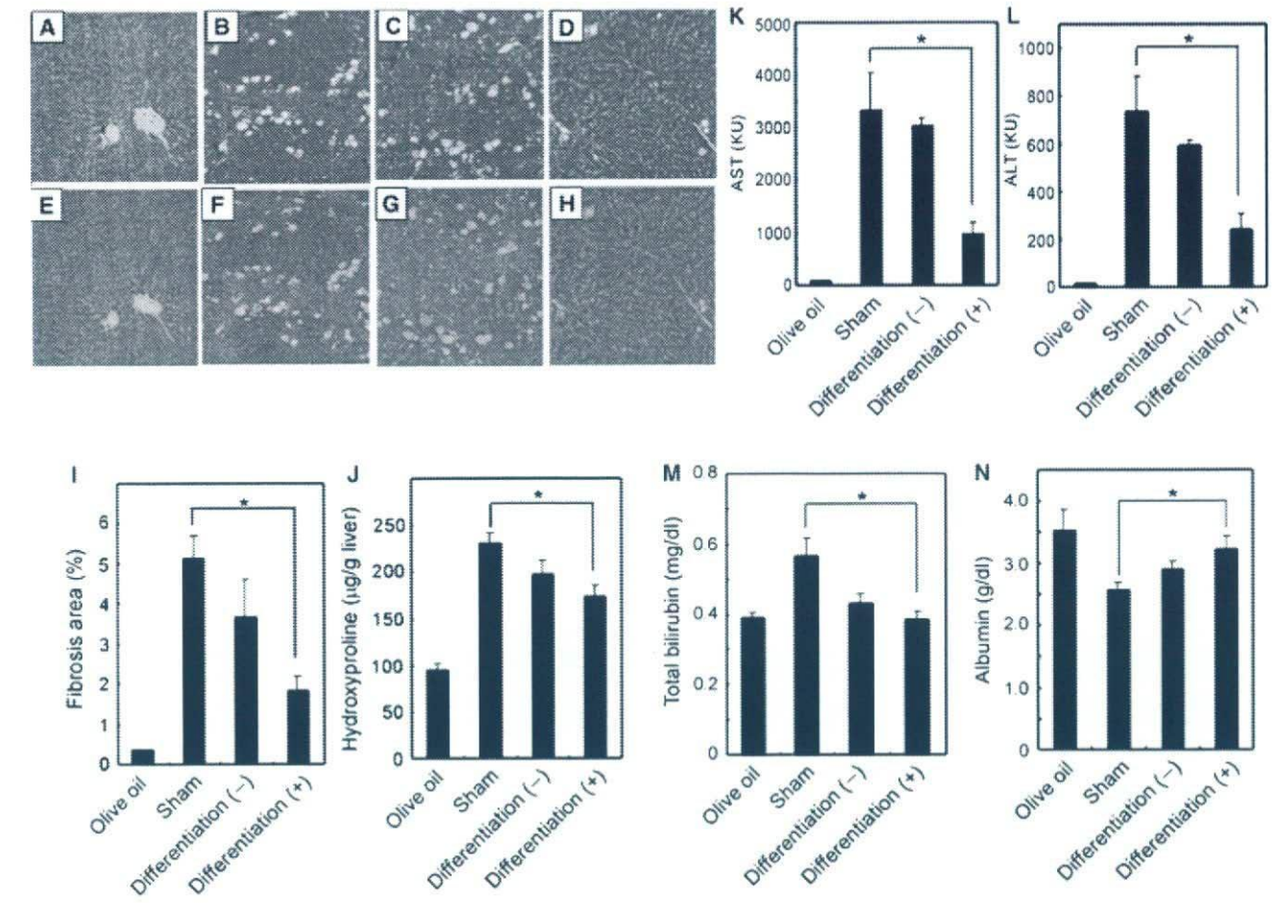

Fig. 6 Suppression of fibrosis and recovery of liver function. Liver sections after staining with Azan (**A–D**) and HE (**E–H**). The CCl_4-injured liver of sham-operated rats (Sham, B and F) and of animals that received transplanted TGPCs with or without hepatic induction (differentiation [+], D and H; differentiation [−], C and G), and the liver of the control animals that received olive oil (Olive oil, A and E). Quantification of liver fibrosis in the CCl4-injured rat liver. The fibrotic area was calculated for five randomly selected liver sections per rat (**I**). Hydroxyproline content in the liver (**J**). AST and ALT levels in rat livers in groups Sham, differentiation (+), and differentiation (−). A significant difference was seen between the values in the Sham ($n = 4$) and differentiation (+) ($n = 3$) groups. KU stands for Karmen unit (**K** and **L**). The total bilirubin (**M**) and serum albumin level (**N**). The findings indicate the recovery of liver functions in CCl_4-injured livers harboring transplanted TGPCs with hepatic differentiation. Values are means ± SD for individual animals. A significant difference was seen between the values in the Sham and differentiation (+) groups. $^*p < 0.05$. TGPC, tooth germ progenitor cells; CCl_4, carbon tetrachloride; AST, aspartate aminotransferase; ALT, alanine aminotransferase, HE, hematoxylin & eosin.

promising strategies of ours including transplantation of novel multipotent TGPCs could help halt malignant progression to HCC in hepatitis patients receiving antiviral treatment. In the future, the surprising potential of TGPCs we evidenced *in vivo* may create new avenues for cell-based therapy to treat other fatal diseases.

References

Akahane, M., Ohgushi, H., Yoshikawa, T., Sempuku, T., Tamai, S., Tabata, S. and Dohi, Y. (1999) Osteogenic phenotype expression of allogeneic rat marrow cells in porous hydroxyapatite ceramics. J Bone Miner Res 14:561–568.

Boyer, L.A., Lee, T.I., Cole, M.F., Johnstone, S.E., Levine, S.S., Zucker, J.P., Guenther, M.G., Kumar, R.M., Murray, H.L., Jenner, R.G., Gifford, D.K., Melton, D.A., Jaenisch, R. and Young, R.A. (2005) Core transcriptional regulatory circuitry in human embryonic stemcells. Cell 122:947–956.

D'Ippolito, G., Diabra, S., Howard, G.A., Menei, P., Roos, B.A. and Schiller, P.C. (2004) Marrow-isolated adult multilineage inducible (MIAMI) cells, a unique population of postnatal young and old human cells with extensive expansion and differentiation potential. J Cell Sci 117:2971–2981.

El-Serag, H.B., Davilla, J.A., Petersen, N.J. and McGlynn, K.A. (2003) The continuing increase in the incidence of hepatocellular carcinoma in the United States. Ann Intern Med 139:817–823.

Ikeda, E., Hirose, M., Kotobuki, N., Shimaoka, H., Tadokoro, M., Maeda, M., Hayashi, Y., Kirita, T. and Ohgushi, H. (2006) Osteogenic differentiation of human dental papilla mesenchymal cells. Biochem Biophys Res Commun 342:1257–1262.

Iohara, K., Zheng, L., Ito, M., Tomokiyo, A., Matsushita, K. and Nakashima, M. (2006) Side population cells isolated from porcine dental pulp tissue with self-renewal and multipotency for dentinogenesis, chondrogenesis, adipogenesis, and neurogenesis. Stem Cells 24:2493–2503.

Kogler, G., Sensken, S., Airey, J.A., Trapp, T., Muschen, M., Feldhahn, N., Liedtke, S., Sorq, R.V., Fischer, J., Rosenbaum, C., Greschat, S., Knipper, A., Bender, J., Deqistirici, O., Gao, J., Caplan, A.I., Colletti, E.J., Almeida-Porada, G., Muller, H.W., Zanjani, E. and Wernet, P. (2004) A new human somatic stem cell from placental cord blood with intrinsic pluripotent differentiation potential. J Exp Med 200:123–135.

Lee, J.Y., Qu-Petersen, Z., Cao, B., Kimura, S., Jankowski, R., Cummins, J., Usas, A., Gates, C., Robbins, P., Wernig, A. and Huard, J. (2000) Clonal isolation of muscle-derived cells capable of enhancing muscle regeneration and bone healing. J Cell Biol 150:1085–1100.

Miura, M., Gronthos, S., Zhao, M., Lu, B., Fisher, L.W., Robey, P.G. and Shi, S. (2003) SHED: stem cells from human exfoliated deciduous teeth. Proc Natl Acad Sci USA 100: 5807–5812.

Nagai, T., Ibata, K., Park, E.S., Kubota, M., Mikoshiba, K. and Miyawaki, A. (2002) A variant of yellow fluorescent protein with fast and efficient maturation for cell-biological applications. Nat Biotechnol 20:87–90.

Ohgushi, H. and Caplan, A.I. (1999) Stem cell technology and bioceramics: from cell to gene engineering. J Biomed Mater Res 48:913–927.

Ohgushi, H., Kotobuki, N., Funaoka, H., Hirose, M., Tanaka, Y. and Takakura, Y. (2005) Tissue engineered ceramic artificial joint—ex vivo osteogenic differentiation of patient mesenchymal cells on total ankle joints for treatment of osteoarthritis. Biomaterials 26:4654–4661.

Oyagi, S., Hirose, M., Kojima, M., Okuyama, M., Kawase, M., Nakamura, T., Ohgushi, H. and Yagi, K. (2006) Therapeutic effect of transplanting HGF-treated bone marrow mesenchymal cells into CCl_4-injured rats. J Hepatol 44:742–748.

Petersen, B.E., Bowen, W.C., Patrene, K.D., Mars, W.M., Sullivan, A.K., Boqqs, S.S., Greenberger, J.S. and Goff, J.P. (1999) Bone marrow as a potential source of hepatic oval cells. Science 284:1168–1170.

Reubinoff, B.E., Pera, M.F., Fong, C.Y., Trounson, A. and Bongso, A. (2000) Embryonic stem cell lines from human blastocysts: somatic differentiation in vitro. Nat Biotechnol 18:399–404.

Sakaida, I., Terai, S., Yamamoto, Nishina, H. and Okita, K. (200 row cells reduces CCl_4-induced l 40:1304–1311.

Seo, B.M., Miura, M., Gronthos, S Brahim, J., Young, M., Gehron S. (2004) Investigation of multi human periodontal ligament. La

Seo, M.J., Suh, S.Y., Bae, Y.C. a ation of human adipose stromal and in vivo. Biochem Biophys F

Tang, X.P., Zhang, M., Yang, X., Differentiation of human umbilica tocytes in vitro and in vivo. Worl

Theise, N.D., Badve, S., Saxena, R ford, J.M. and Krause, D.S. (2(from bone marrow cells in mice ablation. Hepatology 31:235–24(

Theise, N.D., Nimmakayaln, M., C G., Teperman, L., Henegariu, O from bone marrow in humans. H

Thomson, J.A., Itskovits-Eldor, J., Swiergiel, J.J., Marshall, V.S. an stem cell lines derived from 1282:1145–1147.

Toma, J.G., Akahavan, M., Karl, Heider, F., Sadikot, A., Kaplan Isolation of multipotent adult mammalian skin. Nat Cell Biol

Yen, B.L., Huang, H.I., Chien, C.C Shun, C.T., Yen, M.I., Lee, M. lation of multipotent cells from h 23:3–9.

Zipori, D. (2005) The stem state: pl renewal and hierarchy are optior

Zuk, P.A., Zhu, M., Ashjian, P., Mizuno, H., Alfonso, Z.C., Fras rick, M.H. (2002) Human adipos tent stem cells. Mol Biol Cell 13:

Introduction

Tumor necrosis factor (TNF) is as an important immunity-modulating cytokine that is required for human body defense against infectious diseases and carcinogenesis.[1] Excess TNF, however, causes various autoimmune diseases, such as rheumatoid arthritis, Crohn's disease, and ulcerative colitis.[2–4] The relationship between TNF and disease deterioration must be unraveled before effective therapies can be developed. Both TNF receptor (TNFR) types TNFR1 and TNFR2, which induce different cell signaling, must be analyzed to better understand the function of TNF. Experiments with TNFR knockout mice have revealed the individual functions of TNFR1 and TNFR2 against viral infection, microbial pathogens, and tumor immunity.[5–8] The lack of one TNFR type, however, can affect the function of the other receptor type and weaken its signaling because the two receptors work together by crosstalk signaling.[9–11] This issue complicates investigations of the individual roles of TNFR1 and TNFR2, and the analysis of TNFR function. Therefore, many researchers have attempted to activate only one receptor using a receptor-selective TNF mutant that does not impair the function of the receptor.

In the past decade, several receptor-selective TNF mutants, which are useful for functional analysis of TNFRs, have been constructed.[12,13] Traditional point mutation methods, however, are labor-intensive because a large number of candidates must be individually assessed; therefore, it has been difficult to successfully isolate the desired mutants.[14–17] In particular, a receptor-selective TNF mutant with full bioactivity was difficult to develop due to the fact that a region on TNF shares a binding affinity for the two different receptors.[18,19] Furthermore, inadequate mutations cause a loss of affinity for both TNFR1 and TNFR2, which has made it difficult to create novel mutants with high selectivity and full bioactivity.[20] Therefore, functional analysis of TNFR using these mutants has not progressed sufficiently.

We previously developed a modified phage display technique that can be used to create desired functional mutant proteins. Using this technique, we have successfully created many mutants with high bioactivity,[21] high *in vivo* stability,[22] and antagonist activity[23] that are suitable for drug development. The advantage of this method is that it allows us to obtain information about specific functions and associated sequences, which is very useful for determining the structure–function relationship of a specific protein. This information will be useful for improving the design of therapeutic mutants.

In the present study, we used the phage display technique to create novel receptor-selective TNF mutants with full bioactivity. Structural information of the mutants was determined by crystallographic analysis, and structural simulation was used to determine a feasible basis for receptor selectivity. These TNF mutants will be useful tools for analyzing TNFR signaling. An understanding of the structure and sequence of these functional mutants, combined with bioinformatics techniques, can potentially lead to the design of a desired functional protein, peptide, or peptide mimic, and thus accelerate the development of novel strategies for analyzing disease-related proteins, such as TNF, and the development of associated therapies.

Results

Library construction and selection of receptor-selective TNF mutants

To create receptor-specific TNF mutants using our phage display system, we prepared two phage libraries, Libraries I and II. Each library contained six amino acids randomized in a receptor binding site suggested by point mutation analysis and X-ray crystallography (Fig. 1).[16,17,24] For construction of the TNF mutant library, a mutant TNF-Lys(−) gene was used as template for polymerase chain reaction (PCR) mutagenesis.[22] Sequence analysis of randomly selected clones indicated that Libraries I and II contained 8.2×10^6 and 5.6×10^6 independent clones, respectively. For selection from the library, several rounds of affinity panning were performed against human TNFR1 or TNFR2 using BIAcore 3000. Potent binders to TNFR1 or TNFR2 were concentrated in the library through this panning procedure. The monoclonal candidates in each library were picked up for enzyme-linked immunosorbent assay (ELISA) screening to confirm their receptor binding specifi-

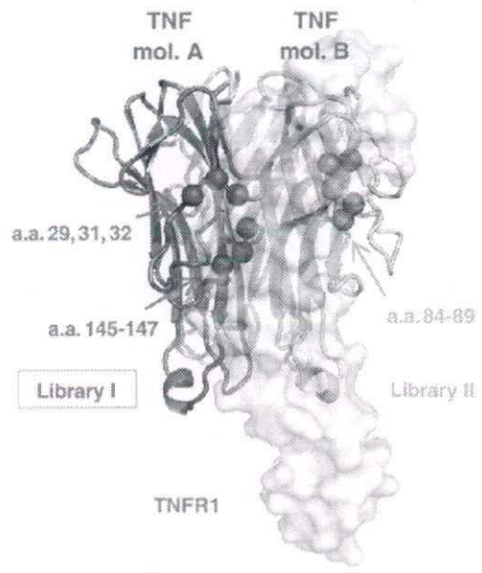

Fig. 1. Positions of randomized residues on the binding interface of the TNF–TNFR1 complex. Mutational residues of Library I (red spheres) and Library II (orange spheres). Green cartoon represents wtTNF. White area represents the surface of the TNFR1 monomer. This binding model structure of the TNF–TNFR1 complex was constructed based on the crystal structure of the LTα–TNFR1 complex (1TNR) and that of wtTNF (1TNF).

Table 1. Substituted residues of TNF mutants from Libraries I and II

			29	31	32	84	85	86	87	88	89	145	146	147
		wtTNF	L	R	R	A	V	S	Y	Q	T	A	E	S
		mutTNF-Lys(−)	—	—	—	—	—	—	—	—	—	—	—	—
TNFR1-selective candidates	Library I (29:32–145:147)	R1-1	I	—	—	—	—	—	—	—	—	—	—	—
		R1-2	Q	—	W	—	—	—	—	—	—	—	—	—
		R1-3	T	G	Y	—	—	—	—	—	—	—	—	—
		R1-4	T	K	Y	—	—	—	—	—	—	—	—	—
		R1-5	T	—	F	—	—	—	—	—	—	—	T	—
		R1-6	K	A	G	—	—	—	—	—	—	—	S	T
	Library II (84:89)	R1-7	—	—	—	S	K	T	—	T	H	—	—	—
		R1-8	—	—	—	S	P	L	—	P	K	—	—	—
		R1-9	—	—	—	S	T	N	—	N	G	—	—	—
		R1-10	—	—	—	T	S	A	—	G	P	—	—	—
		R1-11	—	—	—	T	T	A	—	S	G	—	—	—
		R1-12	—	—	—	T	H	K	—	P	Q	—	—	—
		R1-13	—	—	—	S	K	T	—	S	H	—	—	—
		R1-14	—	—	—	S	S	H	—	R	F	—	—	—
TNFR2-selective candidates	Library I (29:32–145:147)	R2-1	—	—	—	—	—	—	—	—	—	K	D	T
		R2-2	—	—	—	—	—	—	—	—	—	R	T	D
		R2-3	—	—	—	—	—	—	—	—	—	R	E	T
		R2-4	—	—	—	—	—	—	—	—	—	A	D	D
		R2-5	—	—	—	—	—	—	—	—	—	A	N	D

Conserved residues compared with wtTNF are indicated by an em dash (—). Mutated residues in each library are highlighted in gray. Library I included mutated residues 29, 31, 32, and 145–147. Library II contained mutated residues 84–89. R1-1–R1-6 and R1-7–R1-14 were isolated from Libraries I and II, respectively, as TNFR1-selective candidates. TNFR2-selective clones R2-1–R2-5 were isolated from Library I; Library II contained no TNFR2-selective clones.

city. Several clones with TNFR1 or TNFR2 specificity were eventually obtained.

Sequence analysis of receptor-specific TNF mutant candidates

Sequence analysis revealed that we had 14 TNFR1-selective candidates (R1-1–R1-14) and 5 TNFR2-selective candidates (R2-1–R2-5) from Libraries I and II (Table 1). Unfortunately, Library II did not contain any TNFR2-selective mutants. All active TNFR1-selective mutants in Library II retained Tyr87, suggesting that Tyr87 was an essential residue for receptor binding. Analysis of Library I, however, revealed that the mutated and conserved regions of the TNFR1-selective mutants were different from

Table 2. Receptor-selective bioactivities and affinities of TNF mutants

			Relative affinity (% K_d)[a]			Relative bioactivity (% of EC_{50})		
		TNFs	TNFR1	TNFR2	R_1/R_2	HEp2[b]	PC60[c]	R_1/R_2
		wtTNF	100	100	1.0	100	100	1.0
		mutTNF-Lys(−)	108	88	1.2	116	126	0.9
TNFR1-selective candidates	Library I (29:32–145:147)	R1-1	145	121	1.2	492	NT	—
		R1-2	212	32	6.7	436	NT	—
		R1-3	42	18	2.4	343	NT	—
		R1-4	43	3	13.4	447	NT	—
		R1-5	177	2	106.2	582	36	16.2
		R1-6	33	4	8.4	128	<0.07	>1800.0
	Library II (84:89)	R1-7	108	13	8.4	102	NT	—
		R1-8	145	9	16.5	120	173	0.7
		R1-9	175	24	7.4	110	NT	—
		R1-10	149	9	17.0	134	NT	—
		R1-11	219	11	20.4	58	NT	—
		R1-12	51	15	3.5	21	NT	—
		R1-13	51	11	4.6	26	NT	—
		R1-14	46	4	12.0	47	47	1.0
TNFR2-selective candidates	Library I (29:32–145:147)	R2-1	83	112	0.741	12.4	23	0.539
		R2-2	3	143	0.020	0.2	30	0.007
		R2-3	38	225	0.169	2.5	12	0.208
		R2-4	51	572	0.089	6.2	19	0.326
		R2-5	94	324	0.290	13.4	39	0.344

The affinity and bioactivity values are shown as relative values (% wtTNF).
NT, not tested.
[a] Affinity for immobilized TNFR1 and TNFR2 was assessed by SPR using BIAcore 3000.
[b] Human TNFR1-mediated bioactivity was evaluated using a HEp-2 cell cytotoxicity assay. In this assay, HEp-2 cell viability was determined by methylene blue staining. Each value represents the mean±SD.
[c] Human TNFR2-mediated bioactivity was evaluated using PC60-R2 assay. GM-CSF expression by TNFR2-mediated signaling was detected by ELISA. Each value presents the mean±SD.

those of the TNFR2-selective mutants. TNFR1-selective mutants were highly mutated near residue 30 and conserved near residue 140. On the other hand, TNFR2-selective mutants were mutated near residue 140 and conserved near residue 30. This interesting result suggested that the details of the essential binding interface for TNFR1 and TNFR2 differed despite their predicted similar complex forms.[19]

Receptor selectivity and bioactivity of TNF mutants

To investigate the properties of candidate receptor-selective TNF mutants in detail, we prepared recombinant protein using the previously described methods.[21,22] TNF mutants expressed as an inclusion body in *Escherichia coli* were denatured and refolded. Then, active TNF mutants were purified by ion-exchange and gel-filtration chromatography. TNF mutant purity was greater than 90% in sodium dodecyl sulfate–polyacrylamide gel electrophoresis, and all mutants were confirmed to form trimers by gel-filtration analysis (data not shown).

We examined the affinities of these recombinant TNF mutants for TNFR1 and TNFR2 (Table 2). Most of the TNFR1-selective candidates had little affinity for TNFR2 based on surface plasmon resonance (SPR) analysis by BIAcore 3000. In particular, the TNFR1 affinities of R1-2, R1-5, R1-8, R1-9, R1-10, and R1-11 were higher than that of wild-type TNF (wtTNF), despite the loss of their TNFR2 affinities. TNFR1- and TNFR2-mediated bioactivities were assessed by HEp-2 and PC60-hTNFR2 assays, respectively. Interestingly, R1-selective candidates from Library I showed more potent activity via TNFR1 than those from Library II. R1-5 and R1-6 showed superior bioactivity and receptor selectivity. R1-6 was selected as the best overall mutant with greater than 1800-fold selective TNFR1 activity. These mutants were novel because TNFR1-selective mutants with higher bioactivity had not yet been established. Similar studies were performed with the TNFR2-selective candidates. In SPR analysis, these candidates showed higher TNFR2 affinity than wtTNF. Unfortunately, however, none of the TNFR2-selective candidates could sufficiently activate TNFR2 and had less than 40% of the bioactivity of wtTNF.

Next, we performed a competitive binding assay to confirm the details of the TNFR1 selectivity of R1-5 and R1-6—the candidates with the highest selectivity for TNFR1. Competitive affinities were assessed under a certain amount of wtTNF-FLAG, wtTNF fusing FLAG-tag (DYKDDDDK) at C-terminal, as competitor (Fig. 2). Similar to the results of the SPR analysis, R1-5 showed a higher affinity for TNFR1 compared with wild type, and its affinity for TNFR2 was decreased to approximately 10% that for wtTNF, suggesting that R1-5 was a TNFR1-selective mutant. In contrast to the SPR results, however, R1-6 showed a higher competitive affinity for TNFR1, and wtTNF–FLAG binding to TNFR2 was not completely inhibited, even by excess R1-6, which suggested that R1-6

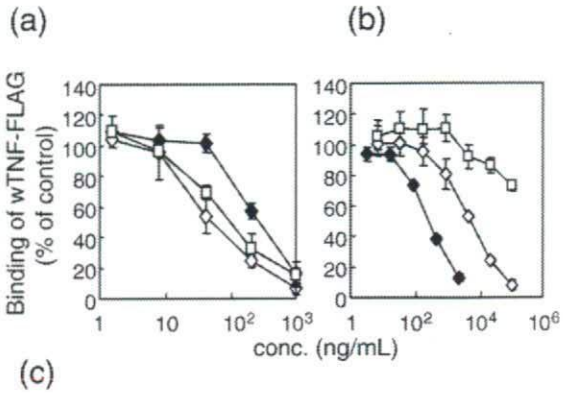

(c)

	TNFR1		TNFR2	
	IC50 (ng/ml)	(%)	IC50 (ngml)	(%)
wtTNF	276.0	100.0	508.1	100.0
R1-5	57.7	478.3	4606.6	11.0
R1-6	105.4	261.9	>100000.0	<0.5

Fig. 2. Competitive binding affinities of TNFR1-selective mutants (R1-5 and R1-6). Competitive affinities were assessed under 50 ng/ml FLAG-tagged wtTNF (wtTNF–FLAG) as competitor. Both (a) TNFR1 and (b) TNFR2 were immobilized. Binding of wtTNF–FLAG was inhibited by serially diluted TNF mutants. Final binding of wtTNF–FLAG was assessed by ELISA. Each value represents the mean±SD. (c) IC_{50} values are given as the concentration of the TNF mutant required to inhibit 50% of the maximal binding of wtTNF–FLAG.

lacked binding potency to TNFR2. Because the TNF binding interfaces to the receptors are known to overlap,[19] TNFR1 selectivity caused by a structural change in the R1-6 surface might provide important information for structure-based drug discovery.

X-ray crystallography of TNFR1-selective TNF mutant R1-6

The structural basis of the TNFR1 selectivity of R1-6 was examined by X-ray crystallography. After establishing crystallization conditions, good-quality crystals of R1-6 were obtained (approximately 0.2 mm×0.2 mm×0.3 mm in size). X-ray diffraction data were collected in SPring-8 (a large synchrotron radiation facility in Harima, Japan). Analysis of these data indicated that the space group is *R*3 and that the lattice constants are $a=135.87$ Å, $b=135.87$ Å, and $c=58.02$ Å (Table 3). The R1-6 structure was further refined using the CNS software suite. The results of model validation using the PROCHECK program indicated that there were 86.9% residues in the most favored regions, 13.1% residues in the additionally allowed regions, 0.0% residues in the generously allowed regions, and 0.0% residues in the disallowed regions.

The overall structures of the R1-6 [Protein Data Bank (PDB) code 2ZJC] and wtTNF (PDB code 1TNF) trimers are also similar and superimpose with an rmsd of 1.21 Å for 428 C^{α} atoms (Fig. 3). The structure of

Table 3. Crystallographic parameters and refinement statistics of the R1-6 crystal

Data collection	
Resolution (Å)	50–2.50 (2.59–2.50)
Cell constants (Å)[a]	135.9, 135.9, 58.0
Space group	*R*3
Measured reflections	74,516
Unique reflections	13,445 (1173)
Completeness (%)	99.9 (85.2)
R_{merge} (%)[b]	0.10 (0.53)
$I/\sigma(I)$	28.9 (4.2)
Refinement statistics	
Resolution (Å)	25.67–2.50
Reflections used	12,060
R_{cryst} (%)[c]	20.1
R_{free} (%)[d]	27.2
Completeness (%)	97.1
Atoms	
Protein; water	3338; 59
rmsd from ideality	
Bond lengths (Å); bond angles (°)	0.009; 1.27
Overall *B*-factor (Å^2)	19.7
B-factor rmsd (Å^2)	
Main-chain bonds; side-chain bonds	0.42; 0.77
Main-chain angles; side-chain angles	0.94; 1.48
Ramachandran plot statistics	
Most favored regions (%)	86.9
Additionally allowed regions (%)	13.1
Generously allowed regions (%)	0.0
Disallowed regions (%)	0.0

Values in parentheses are those for the outer shell.

[a] Cell constants are *a*, *b*, and *c*.

[b] $R_{merge} = \sum |I - \langle I \rangle| / \sum \langle I \rangle$, where I is intensity of the observations. R_{merge} in the last shell is high because of the anisotropic mosaicity of the crystal.

[c] $R_{cryst} = \sum ||F_o| - |F_c|| / \sum |F_o|$, where F_o and F_c are the observed and calculated structure factors, respectively.

[d] R_{free} is calculated as for R_{cryst}, but for the test set comprising reflections not used in refinement. The overall *B*-factor was calculated after TLS parameter analysis (TLSANL) using Refmac.

each monomer is similar to each other (rmsd of 0.98–1.12 Å for 140 C^α atoms). Especially, the structures of the β-sheet in each monomer are essentially the same (rmsd of 0.31–0.42 Å for 63 C^α atoms). These features have been found in the wtTNF trimer.[25]

The R1-6 loop structure near mutational residues 31 and 32 is different from that in wtTNF (Fig. 4). This loop structure between monomers is not different (wtTNF: rmsd of 0.61–0.72 Å for 11 C^α atoms; R1-6: rmsd of 0.39–0.91 Å for 11 C^α atoms) (Fig. 4a and b). However, they are clearly different between wtTNF and R1-6 (Fig. 4c). This structural change is thought to be caused by R32G mutation from a sterically bulky arginine residue to a flexible glycine residue. Because this region is close to the TNFR surface, such a structural change in the C^α chain could influence receptor binding. Additional TNF–TNFR docking simulation studies are discussed below.

Discussion

We recently developed the technology to create functional mutant proteins with high bioactivity, high *in vivo* stability, and antagonistic activity.[21–23] Here, we attempted to establish fully bioactive receptor-selective TNF mutants for functional analysis of TNFR1 and TNFR2 using our optimized phage display system. We constructed TNF mutant libraries (Libraries I and II) in which six residues near the receptor binding region were randomized (Fig. 1). From these libraries, we screened for TNFR1- or TNFR2-selective binders, and isolated receptor-selective candidates (Table 1). Despite the successful isolation of TNFR2-selective binders, the TNFR2-selective candidates obtained could not sufficiently activate TNFR2. This result suggested that the production of TNFR2-selective mutants was very rare in our library and that an improved panning method was necessary.

One advantage of our phage-display-based technique is that it can be used to obtain the sequence information of many mutants (Table 1). Tyr87 of TNF was conserved in all mutants obtained from Library II. This residue is highly conserved throughout the TNF superfamily, such as in LTα, LTβ, and LIGHT, and site-directed mutagenesis of the Tyr87 residue of TNF results in a dramatic loss of its biologic activity and its affinities for both TNFR1 and TNFR2.[17] In addition, Tyr87 replacement in antagonistic TNF causes unstable receptor binding and loss of receptor activation in our report.[23] These findings together indicate that Tyr87 is an essential residue for receptor signaling and receptor complex stability.

TNFR1-selective mutants had mutations near residue 30 and conserved residues near residue 140. In contrast, TNFR2-selective mutants had mutations near residue 140 and conserved residues near residue 30. These findings support those of previous point mutation analyses[15–17] and suggest that our phage-

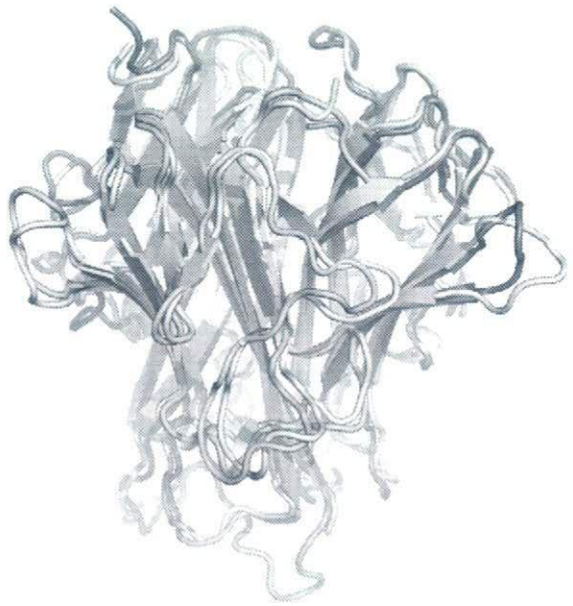

Fig. 3. Overall structure of wtTNF and R1-6. Merge image of previously reported wtTNF structure (green; 1TNF) and refined structure of R1-6 (white; 2ZJC). The flexible loop containing residues 100–110 shown at the bottom of the figure was disordered in the R1-6 structure.

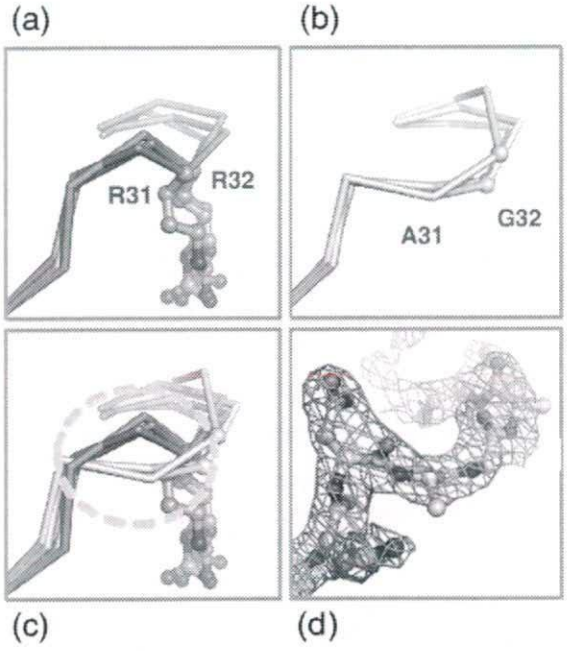

Fig. 4. Structural difference in receptor binding loop between wtTNF and R1-6. Each TNF monomer was superimposed using the CCP4i program. Details of the receptor binding loop, including residues 31 and 32, are shown in these figures. (a) Loops of wtTNF monomers (green); (b) loops of R1-6 monomers (white); (c) merged image of the loops of wtTNF and R1-6; (d) $2F_o - F_c$ map contoured at 1.0σ of R1-6 loop (pink mesh). The different C^{α} chains are highlighted by the dashed orange circle in (c).

display-based technique can be used to rapidly gather important information about the function–sequence relationships determined by long-term point mutation analysis. In the present study, we successfully isolated mutants that retained TNFR affinity from a huge phage library containing over a million repertoires. Most of the mutants in the library had no TNFR affinity and were therefore discarded through this selection step. This finding may indicate that the mutational residues in these unbound clones diminish TNFR affinity. This method may be useful for examining the function, capability, and sequence–function relationship of unknown cytokines and proteins.

Using these receptor-selective candidates, we expressed recombinant proteins and estimated their bioactivities and affinities for TNFR1 and TNFR2. R1-6, the most highly TNFR1-selective mutant, bound and activated TNFR1 efficiently despite the loss of its affinity for TNFR2. X-ray crystallography of R1-6 revealed that the crystal structure of R1-6 was a trimer (similar to wtTNF), and no other salient differences in the overall structure were observed. Superimposition of wtTNF and R1-6 sequences, however, revealed that the C^{α} of the receptor binding loop near residue 30 was partially different (Fig. 4). This change might influence the receptor binding mode of R1-6. We further used the superimposition program to perform docking simulations with TNF and TNFR1 based on the crystal structure of the LTα–TNFR1 complex (PDB code 1TNR).[18]

Based on the model wtTNF–TNFR1 complex, Arg31 of TNF would interact electrostatically with Glu56 of TNFR1. The main chain of TNF was too close to His69 of TNFR1, however, potentially causing potential steric hindrance (Fig. 5a). On the other hand, a structural change in the loop in R1-6, however, was thought to solve this problem (Fig. 5b). Arg32 of wtTNF associated with Ser72 of TNFR1 (Fig. 5a). In the R1-6 structure, however, this role of Arg32 was thought to be compensated for by Lys29 (Fig. 5b). This speculation was supported by the crystal structure of the LTα–TNFR1 complex.[18] The position of Lys29 in R1-6 corresponded to that of Arg46 in LTα interacting with Ser72 of TNFR1 by hydrogen bonding. This interesting "compensating role of an amino acid" would be difficult to induce using single point mutation methods, which is another advantage of our modified phage display technique.

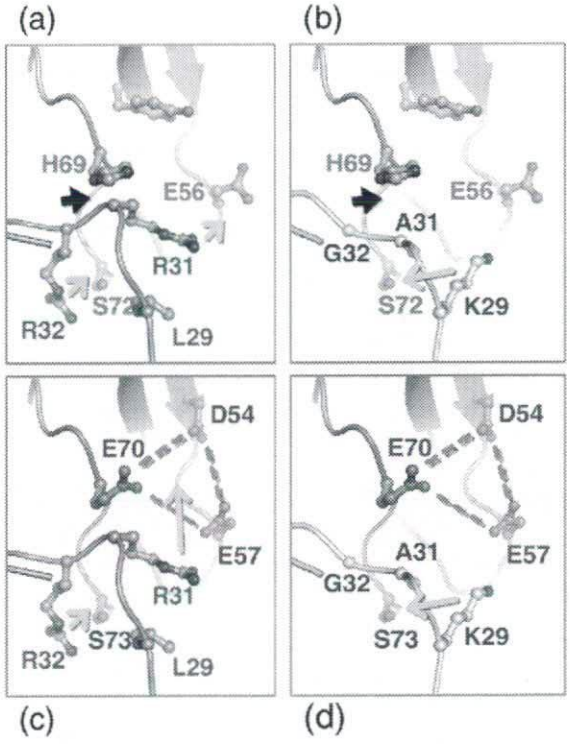

Fig. 5. Model of TNF binding to TNFR1 and TNFR2. Receptor binding interfaces of (a) wtTNF–TNFR1 (green–red); (b) R1-6–TNFR1 (white–red); (c) wtTNF–TNFR2 (green–blue); and (d) R1-6–TNFR2 (white–blue). The TNF–TNFR1 model complex was constructed from 1TNF (wtTNF) and 1TNR (LTα–TNFR1 complex). The predicted TNFR2 structure was constructed by side-chain mutation using the O program. In this simulation, the side chains of each structure were rotated to fit the predicted interaction. Stable structures of these rotamers were constructed using the O program. Steric hindrance might have occurred between His69 of TNFR1 and Arg32 of wtTNF in (a) (black arrowhead). Potential interactions are indicated by orange arrows. A cluster of anionic charged residues (Asp54, Glu57, and Glu70) is highlighted by a broken red line.